New genetic mouse models for neurodegenerative diseases: Contribution of noradrenaline to Alzheimer's disease pathogenesis and creation of a new genetic model for Parkinson's disease.

Dissertation

for the award of the degree

"Doctor of Philosophy"

Division of Mathematics and Natural Sciences

Submitted by

Ana C. Martinez Hernandez

from Mexico City

Göttingen 2011

Prof. Dr. Gregor Eichele (Reviewer)

Genes and Behavior Department, Max Planck Institute for Biophysical Chemistry

Prof. Dr. med. Mathias Bähr

Department of Neurobiology, University of Göttingen

Prof. Dr. Ahmed Mansouri

Molecular Cell Differentiation Group, Max Planck Institute for Biophysical Chemistry

Prof. Dr. Markus Zweckstetter

Department of NMR-based Structural Biology, Max Planck Institute for Biophysical Chemistry

Prof. Dr. Klaus-Armin Nave

Department of Neurogenetics, Max Planck Institute for Experimental Medicine

Prof. Dr. André Fiala

Department of Molecular Neurobiology of Behaviour, University of Göttingen

Declaration

Herewith, I confirm that I have written the present PhD thesis independently and with no other sources and aids than quoted.

Göttingen, September 2011 Ana Martinez Hernandez

Table of Contents

Summary

Neurodegenerative diseases are among the most devastating diseases for which there are no cure to date. The greatest risk factor is advancing age. A common feature of these disorders is the toxic aggregation of a peptide particle. In Alzheimer's, extracellular Aβ plaques are the pathological hallmark, while in Parkinson's (PD), intraneuronal α synuclein inclusion bodies (Lewy bodies) mark pathology. This study will focus on the genetic approach to address open questions in these diseases which current genetic models have been unable to do.

Although Aβ plaques are the hallmark of AD, the first asymptomatic stage precedes cognitive impairment by many years. Degeneration of the locus coeruleus (LC) is an early feature of AD. LC degeneration is preferential to rostral regions, which project to the cortex and hippocampus. These regions are also first affected in AD and are important for memory and learning. The LC nucleus has ubiquitous projections reaching all areas of the brain and providing the sole noradrenergic innervations to the cerebral, limbic and cerebellar cortices. LC has global functions. It is involved in general arousal, attention, vigilance and sensory processing, among others. The LC has also been implicated in cognitive functions such as synaptic plasticity, memory, adaptive gain and optimal task performance.

Although many genetic AD mouse models exist, early LC cell loss is not recapitulated in these models. The exact contribution of LC loss to AD has remained elusive. Previous attempts to address this question, relied on either physical disruption of LC cells – through surgical intervention –, or the used of the neurotoxin N-(2-chloroethyl)-N-ethyl-2-bromobenzylamine (DSP-4) to chemically ablate LC cells. These procedures are invasive and unspecific. They can elicit compensatory responses to treatment and acute injury. We found a genetic approach to be more suitable to address the functional consequences of LC loss in AD pathogenesis and disease progression. To that end we crossed LC-deficient Ear2 (-/-) mice to double transgenic APP/PS1 mice, a model for AD.

We observed a 56% reduction in the number of Th(+) LC cells in Ear2 (-/-) mice, whether or not APP/PS1 were present. By 6 months of age, extent of plaque deposition seemed not affected by

NA deficiency. Noradrenaline (NA) levels correlated with the degree of LC innervation and APP/PS1 had no effect on NA levels. NA reduction in Ear2 (-/-) young mice was greatest in areas highly innervated by the LC. Olfactory bulb, frontal cortex and hippocampus lost 65, 53 and 70% NA, respectively. Cerebellum, with less LC input, lost 32%. APP/PS1 had no effect on NA levels. Regions most affected are important for memory and learning and affected in AD. The Morris water maze and electrophysiological recordings revealed a spatial learning and LTP impairment in both, Ear2 (-/-) as well as in APP/PS1 mice; but, the combination of these was most detrimental. LTP impairment was not associated to a short-term plasticity deficit and paired-pulse facilitation (PPF) was unaffected by NA reduction. Furthermore, the ratio of PPF remained unchanged before and after LTP, suggesting presynaptic terminals to be unaffected. Most importantly, cognitive impairments of Ear2 (-/-) were controlled by LC NA and treatment with the NA-agonist L-Threo DOPS restored cognitive functions. Under an AD-like background, the most detrimental cognitive impairment by NA deficiency and the partial restoration of cognitive function by supplementation of NA, argued for NA as a modifier of AD pathology.

LC size was not affected by age or the chronic long-term deficiency of NA. NA reduction in aged Ear2 (-/-) mice was 76, 60, 75 and 51% in the olfactory bulb, frontal cortex, hippocampus and cerebellum, respectively. These represented higher losses that those seen at 3 months of age, indicating that chronic NA deficiency was accentuated with age. Comparing NA content of aged (1 year) vs. young (3 mo) mice revealed no NA loss in wt mice, an approx. 25% NA decrease in Ear2 (-/-) or APP/PS1 mice, and a NA reduction almost twice as large in the Ear2 (-/-)/APP/PS1. We concluded that in our wt mice there was no aging effect to NA levels in the brain. Long-term overexpression of APP/PS1 or long-term chronic NA deficiency seemed to deregulate the NAergic system. More importantly, the long-term chronic NA deficiency in a diseased environment is most detrimental to NAergic deregulation, which resembles early stages of AD.

In conclusion, our model mimicked all features we have aimed to recapitulate. Specifically, we confirmed in our model at pre-plaque stages LC cell loss, decreased levels of NA, higher cognitive impairments and an AD-like phenotype that was reinforced with age. This features made our model a more suitable one to study early stages of AD pathogenesis and disease progression. In doing so, we found NA to be a disease modifying factor of AD-like pathology and we propose it to be a promising therapeutic to partially alleviate early cognitive functions in MCI or early AD.

In PD, α-synuclein (SNCA) is the main component of Lewy bodies aggregating in neurons of the dopaminergic (DAergic) system in the brain. Existing models of PD and patients with duplications or triplications of SNCA have shown that PD is gene-dosage dependent. Current genetic SNCA models of PD are mostly based on overexpression. These models do not recapitulate all features of PD. For example, cell loss is not always achieved. Structural biology work and *in-vivo* testing has shown a mutant SNCA carrying three substitutions to a proline (TP-SNCA) to have reduced fibril formation, increased amounts of soluble oligomers and higher toxicity. Our aim was to generate a novel genetic model of PD to test the toxic properties of TP-SNCA in the mouse.

Here we describe the cloning strategy used to generate the targeting vector of a new knock-in / knock-out, conditional mouse model that we termed SNCA to P3. These mice are engineered to express wt human SNCA in the endogenous mouse *Snca* locus in a conditional manner. Their progeny will switch to express TP-SNCA exclusively in the DAergic neurons, upon their mating to the DATcre line. Importantly, our model is not based on overexpression. By targeting the start codon of the murine gene, we disrupt its expression and utilize its endogenous promoter. This will ensure endogenous levels of expression of wt Human SNCA. Our model has spatio-temporal regulated expression of the mutant SNCA. This provides an additional level of specificity because expression of the toxic TP-SNCA will be directed and restricted to DAergic cells. So far, 2 positive ES cell clones have been identified and blastocyst injection will follow. The spatio-temporal and dosage-regulated expression makes our model a suitable one to study the toxic properties of TP-SNCA. Additionally, the full value of our model relies on its potential to target different cell populations to be able to investigate the contribution to PD pathology of TP-SNCA's toxic expression.

Chapter 1. Introduction

Neurodegenerative disorders comprise a heterogenous group of chronic and progressive diseases such as Huntington's, Parkinson's, Alzheimer's and Prion disease as well as tau pathologies [1]. These disorders are among the most devastating diseases for which we currently have not cure. A common feature in these disorders is the toxic aggregation of a protein particle and they are thus often referred to as aggregopathies. Except for Huntington's disease, which is acquired in an entirely genetic manner, most aggregopathies are complex disorders occurring sporadically, but in some instances, are caused by inheritance of mutated genes [1]. This study will focus on the two most prevalent neurodegenerative disorders [2], namely Alzheimer's disease and Parkinson's disease.

1.1. Alzheimer's Disease

1.1.1. Prevalence of the disease

Alzheimer's disease (AD) is a devastating, progressive and terminal neurodegenerative disease with no cure to date. AD results in a progressive decline of cognition and is the most common cause of dementia [3,4]. Over 36 million people are affected with dementia worldwide [5]. The greatest risk factor for AD is advancing age and most people affected with the disease are aged 65 years or older [6]. Among the top 10 causes of death in the US, AD is number 6 [7]. AD is the only disease in the top 10 list that cannot be prevented, cured or even slowed [3]. Furthermore, while death rates for most major diseases have declined from 2000 to 2008, deaths from AD have risen by 66% [3]. In light of these alarming statistics, it is clear that AD has put an impressive economical and social burden on health care systems and societies around the globe. An aging population is on the rise and the economical burden of AD will continue to increase as well [6].

1.1.2. Description of the disease

AD causes the progressive loss of memory and other intellectual abilities. Symptoms include disorientation, confusion, mood and behavior changes, and difficulty in speaking, swallowing and

walking [8]. Disease progression is categorized into 7 stages by Dr. B. Reisberg [9]. The first stage (of no impairment) is completely asymptomatic and it is thought to begin 10 years or more before the patient first experiences any of the typical cognitive symptoms of AD [3,9]. Stages 2 and 3 involve respectively, very mild and mild decline of cognitive functions [9]. Subsequent stages involve the progressive impairment from moderate to moderately severe to very severe decline (stages 4 to 7) [9]. A combination of mixed pathologies is common in older persons with dementia and at early stages of dementia it is difficult to discern them apart [10]. Mild cognitive impairment (MCI) is an established risk factor for AD. MCI is a condition in which essential cognitive abilities are impaired severely enough to be noticed by others and detected by cognitive testing, yet subjects are not demented, nor does this impairment affect the their daily life [3,11]. MCI is often considered the earliest clinical sign of probable AD because the pathological basis of MCI is similar to that of AD pathology [10].

1.1.3. AD pathology

Biochemically, AD pathology is characterized by the accumulation of senile plaques, neurofibrillary tangles, neuronal loss and changes in choline acetyltransferase activity [10,12]. Earliest damage in AD occurs in the entorhinal cortex, hippocampus and basal forebrain, which are regions with critical roles in memory [8,12] . Damage coincides with sites of plaque deposition [8,13].

Senile plaques aggregate extracellularly and contain Amyloid-β (Aβ) amd neurofibrillary tangles that are intraneuronal aggregates composed of hyperphosphorylated forms of the microtubule-associated protein tau [12,14,15]. These two – Aβ and tau – are the two hallmark proteins in AD [16]. Aβ is produced by the processing of the amyloid precursor protein (APP) through the amyloidogenic pathway [17].

1.1.4. APP processing pathways and mutations known to cause familial AD

The amyloid precursor protein (APP) is a type I transmembrane protein consisting of 695- 770 amino acids. Endoproteolytic and sequential cleavage of APP can occur through two distinct pathways to release either Aβ (amyloidogenic pathway), or p3, a non-pathogenic peptide (non-amyloidogenic pathway) (as reviewed in [18,19,20], Fig. 1). Most APP is processed via the non-amyloidogenic pathway, where the initial enzymatic cleavage is mediated by α-secretase. Cleavage by α-secretase occurs within the Aβ region and thus the formation of Aβ is precluded. The first cleavage results in the release of an extracellular, soluble APP fragment (sAPPβα) of ~110 -120 kDa and a remaining C-terminal fragment of 83 amino acids in length (C83). Subsequently, C83 is cleaved by a γ-secretase enzyme complex to release a small, non-toxic p3 peptide (3 kDa) and a C-terminal fragment, the amyloid intracellular C-terminal domain (AICD). In the amyloidogenic pathway, APP is first cleaved by β-secretase. Cleavage by β-secretase releases an extracellular sAPPβ and the 99 amino acid-long C-terminal fragment (C99) is retained within the membrane. C99 is subsequently cleaved by a γ-secretase enzyme complex to release Aβ and AICD.

The γ-secretase complex is formed by the enzymes presenilin-1 (PS1), presenilin-2 (PS2), nicastrin and Aph-1 [21].

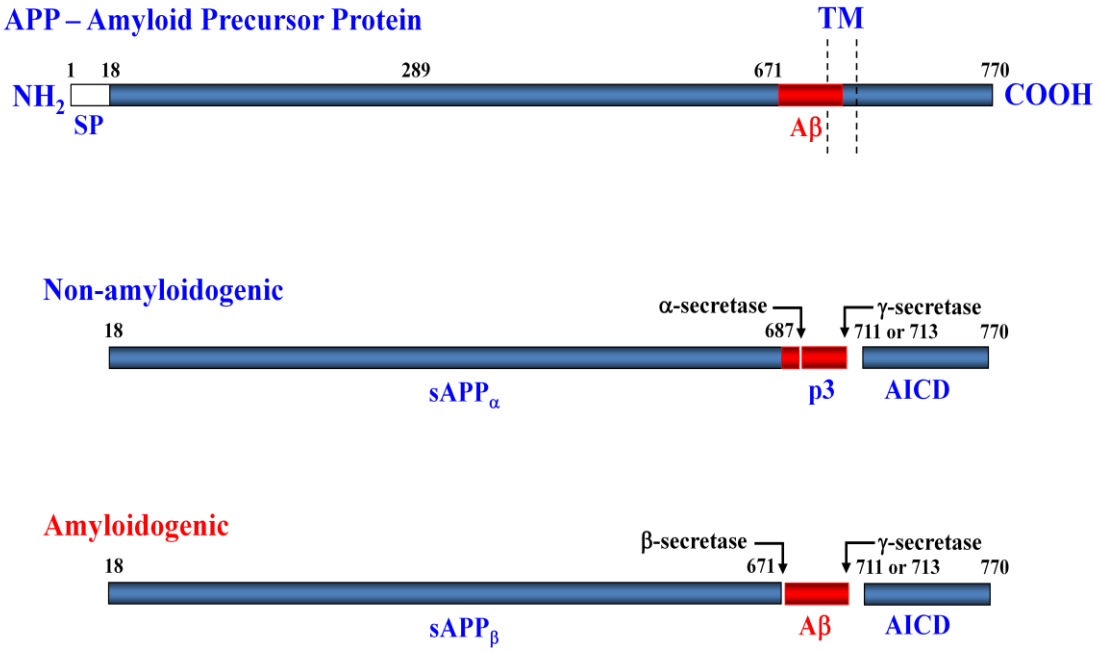

Fig. 1. APP processing pathways. Amyloid-beta (Aβ) is produced by the proteolytic cleavage of its precursor protein, the amyloid precursor protein (APP). APP is a type I transmembrane protein of 695- 770 amino acid residues. APP can undergo two distinct processing pathways to release either the non-pathogenic p3 peptide (through the non-amyloidogenic pathway), or the Aβ peptide (through the amyloidogenic pathway). In the prevalent non-amyloidogenic pathway, APP is fist cleaved by α-secretase within the Aβ region, thus preventing its formation, and leading to the extracellular release of an α-cleaved, soluble APP fragment ($sAPP_{\alpha}$). Additionally, the remaining 83 amino acid-long carboxy-terminal fragment (C83) is further cleaved by the γ-secretase enzyme complex. This generates a small 3 kDa, non-toxic p3 peptide and an APP intracellular C-terminal domain (AICD). Alternatively, in the amyloidogenic pathway, the first enzymatic cleavage is mediated by β-secretase to release an ectodomain ($sAPP_{\beta}$) and retaining the 99 amino acid carboxy-terminal (C99) within the membrane. C99 is further cleaved by the γ-secretase enzyme complex to release Aβ and AICD. SN, Signal peptide; TM, Transmembrane region. Modified from Cam and Bu, 2006.

Specific mutations in the *APP* or the *PS1* genes are known to cause early-onset, familial AD. Some of the mutations, segregating in an autosomal dominant fashion, have been exploited in the generation of genetic models to mimic AD pathology.

In the *APP* gene, among the most frequently used mutations to generate transgenic models of AD are the Swedish and London mutations. The former refers to two missense mutations just prior to the Aβ N-terminus at positions 594 and 595 substituting K → N and M → L, respectively, found in a family of Swedish origin [22]. The latter refers to the V717I substitution found in a family of British origin [23].

In *PS1* many mutations concentrate in and around the transmembrane regions of the protein [24,25,26]. Transgenic AD models carrying mutated versions of the *PS1* gene often target mutations shown to produce a most aggressive AD-like phenotype.

Mutations in the *APP*, *PS1* and *PS2* genes account for most of the familial early-onset cases of AD by enhancing the production of pathological Aβ (42 amino acids long) and favoring aggregation [27].

1.1.5. Neuronal loss and degeneration of the Locus Coeruleus

Another pathological feature of AD is neuronal loss. Post-mortem analysis of definitive AD brains has shown extensive neuronal loss in cortical and hippocampal regions and in the noradrenergic nucleus Locus Coeruleus (LC)[4,28,29]. LC cell numbers are reduced by approx. 55% in AD and 78% in Parkinson's disease patients [29]. LC loss results in decreased noradrenaline (NA) levels in the forebrain regions in AD [4,13,30,31,32]. Furthermore, reduction of NA in the cortex [4] or LC cytophathology [33] in AD brains correlates with cognitive impairment. Additionally, LC loss correlates with disease duration [29,34] and severity of cognitive decline [35].

Although LC loss exists in both Alzheimer's and Parkinson's disease (PD), there are disease-specific patterns of LC cell loss. Cell loss in PD ranged from 30 to 90% in the mildest and most severe instances, respectively. Notably, the pattern of cell loss followed a rostral to caudal fashion [29]. In AD, however, the extent of cell loss was positively correlated to the duration of dementia [29,34]. Patients with a 1.5 to 2 years history of dementia had a 48 to 69% LC cell loss, while 58 to

89% LC cell loss was observed for brains of patients with 3 to 8 years of dementia. Most demented patients lost 81 % LC cells, whereas least demented ones exhibited <20% cell loss. The pattern of LC cell loss in AD was greatest rostrally, and caudal LC cells seemed to be spared [29]. Rostral LC neurons project to the cortex, hippocampus and forebrain, while ventrocaudal neurons innervate the spinal cord and cerebellum preferentially. In AD, there seems to be a sparing of cells projecting to the latter regions [29]. Notably, former regions are relevant for learning and memory and initially also most affected by plaque deposition in AD.

Importantly, degeneration of the LC has been detected at early stages of AD [29,33]. Emerging data present evidence for LC loss to begin several years to decades before the clear manifestation of cognitive impairments and dementia [36,37]. Thus, LC degeneration has been proposed as an early feature of MCI or AD and as a factor mediating the onset of cognitive impairment [33,38]. Treatment after definitive plaque deposition might be too late in the pathogenic process of AD for an agent to revert the effects of a long-term toxic environment to any significant level. It is thus important to investigate early stages of AD. These are potentially the most promising phases to develop successful strategies to manage and treat AD. Not surprisingly, pharmaceutical companies and research consortia, like the AD Cooperative Study, are focusing on MCI patients for large treatment trials [11].

Toxin-induced degeneration of LC neurons exacerbates AD pathology in models of AD providing evidence for the involvement of LC loss in AD progression. Selective ablation of LC neurons with the neurotoxin DSP-4 in mouse models of AD promoted pathogenesis by increased glial inflammation, amyloid plaque deposition, cortical and hippocampal neurodegeneration, and ultimately neuronal loss [38,39].

1.1.6. Description of the Locus Coeruleus

1.1.6.a. Anatomical description of the Locus Coeruleus

The LC is a nucleus located in the dorsal pons [40]. Immunohistochemical and computer-aided three dimensional reconstructions of the adult human LC show it as a continuous column of approximately 15 mm in length, extending rostrocaudally in the upper lateral pontine central gray [41,42,43]. The LC nucleus of young adult humans is composed of 45 000 to 65 000 neurons [29,42,44].

The concept of an aging component to reduce the number of LC cells through life is slowly more accepted; however, reports are still inconclusive. In humans, using computer-assisted mapping of immunoreactive neurons and three-dimensional reconstruction the number of LC neurons declines by 25% with age [13,44]**.** NA concentration was reduced between the fourth and ninth decades in humans [13]. However, using unbiased stereological methods, no change in cell number or size is seen in the LC of older as compared to young individuals [45]. Methodological differences, exact delineation of LC proper cells and the assumption-based nature of conventional sampling and estimation techniques have been suggested as possible explanations for the discrepancy. In rats, Hervonen and colleagues have analyzed the LC of young and aged rats in several occasions and found no LC cell loss due to age [46,47,48].

1.1.6.b. Projection areas of the Locus Coeruleus

The LC is a unique nucleus in that is has the most divergent and ubiquitous projections throughout the central nervous system [43]. LC projections reach almost every region of the brain (Fig.2), with the exception of the basal ganglia [49]. While other noradrenergic cell groups exist, the LC (cell group A6) is considered to be the main NA producer in the brain [13,49,50]. LC neurons provide the sole noradrenergic innervation of the cerebral, limbic and cerebellar cortices [43]. LC projections reach all cerebral cortices. Among the thalamic nuclei and limbic structures receiving input from the LC are the amygdala, hippocampus and septum. LC efferents innervate also the brainstem [13,49]. Through a high degree of axonal branching single neurons from the LC can innervate multiple regions that are remotely located within the brain, from cortex to brain stem or cerebellum [29,49].

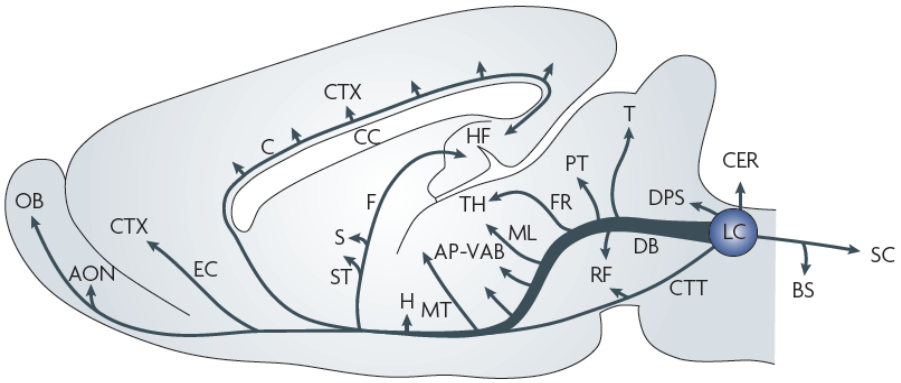

Fig. 2. Schematic representation of locus coeruleus (LC) noradrenergic projections. The LC (A6), located in the dorsal pons, is the main brain source of noradrenaline (NA) projecting mainly to the ipsilateral forebrain. LC projects to the entire cortex. Also, thalamic nuclei and limbic structures, including the amygdala, hippocampus and septum receive LC projections. Owing to their highly axonal branching, a single LC neuron can innervate multiple brain regions that are distant from one another. Notably, the only region devoid of LC input is the basal ganglia. Abbreviations: AON, anterior olfactory nucleus; AP-VAB, ansa peduncularis–ventral amygdaloid bundle system; BS, brainstem nuclei; C, cingulum; CC, corpus callosum; CER, cerebellum; CTT, central tegmental tract; CTX, cortex; DB, dorsal bundle; DPS, dorsal periventricular system; EC, external capsule; F, fornix; FR, fasiculus retroflexus; H, hypothalamus; HF, hippocampal formation; ML, medial lemiscus; MT, mamillothalamic tract; OB, olfactory bulb; PT, pretectal area; RF, reticular formation; S, septum; SC, spinal cord; ST, stria terminalis; T, tectum; TH, thalamus. Modified from Sara, 2009, Nat Rev Neuroscience.

1.1.6.c. Functional description of the Locus Coeruleus

Because of its ubiquitous projections, the LC has been proposed to have global functions [29]. The LC is involved in general arousal, attention, stress, anxiety, affective disorders, vigilance, and sensory processing, [as reviewed in [30,49,50]]. It has also been implicated in cognitive functions including synaptic plasticity, memory, decision making, performance facilitation, adaptive gain and optimal performance [as reviewed in [49,51]]. Pharmacological studies have provided evidence for LC NA to modulate memory formation (through input to the amygdala and hippocampus) and in attention and working memory functions (through frontal cortex innervations). Likewise, electrophysiological analyses of LC neurons show a clear relation between LC neuronal activity and cognitive behavior ([49].

1.1.6.d. Neurochemical description of the Locus Coeruleus

Most LC neurons synthesize and transport NA. Although, NA is best known for its function as a classical neurotransmitter, locally diffusing NA also has anti-inflammatory properties by negatively regulating the transcription of inflammatory genes in astrocytes and microglia. [52]. Inflammation has been extensively linked to AD pathology because Aβ toxicity to cells is mediated by neuroinflammation, among several other mechanisms[53]. Furthermore, Aβ is known to activate the classical pathway complement cascade [54]. Congruently, sites of Aβ plaque deposition are also sites where inflammation is detected [35]. We have recently shown that toxin-induced degeneration of the LC induced inflammation and contributed to reduce Aβ clearance [55].

Although the LC is considered the main source of NA in the brain, LC cells do not synthesize NA exclusively. Subsets of LC neurons produce and transport also other neuromodulators. Among those are brain-derived neurotrophic factor (BDNF) [56], neuropeptide Y (NPY) [57], galanin [57], enkephalin and cocaine-and amphetamine-regulated transcript (CART) [58].

Our lab had previously generated the Ear2 knock-out mutant mouse [59]. Under a genetic hybrid background, adult Ear2 (-/-) mice lack more than 70% LC neurons. Agenesis is preferential to the dorsal division of the LC, which projects to cortical areas [59]. Ear2 (-/-) mice develop otherwise normal, are born alive and are fertile. Other features of Ear2 mutant mice are deregulation in circadian rhythmicity and impaired nociception [59].

1.1.7. Current genetic mouse models of AD

With molecular biology becoming a standard procedure, many genetic murine models of AD became available within the last few decades. As previously discussed (see section: “APP processing pathways and mutations known to cause familial AD” above), most genetic models have attempted to mimic the disease using mutations known to cause early-onset familial AD. Most of these mutations [27], and thus genetic models, involve the *APP, PS1, PS2* and tau genes

either alone or in combination [30]. However, other AD-associated genes have also been used in the creation of novel models seeking to recapitulate the disease more faithfully. Among these, models involving ApoE, tau protein, BACE (γ secretase) or TGF-β1 (a cytokine) are available [for review see [60]].

A wealth of genetic mouse models exists to date. There are for example knock-ins, knock-outs, single-, double- or triple mutants. And many models now carry a combination of two or more variant genes. The overwhelming majority of genetic models available are transgenic. Typically, a mutant variant of the gene(s) is under the expression control of a neuronal-specific strong promoter, the prion protein (PrP) or Thy1 promoters are examples, to drive elevated and directed expression of the transgene(s).

Among the many models available, most transgenic APP mice carry the Swedish mutation, alone or in combination with different mutations in PS1. For example, the APP/PS1KI model expresses a human APP (751 amino acids long) with the Swedish and London mutations together with 2 mutations in PS1 (M233T and L235P). APP is under the control of a Thy1 promoter and PS1 under the endogenous mouse PS1 promoter (knock-in)[61,62]. Although these mice seem normal at 2 months of age, at the age of 6 months a dramatic, age-dependent manifestation of AD-like features begins. These include Aβ plaque deposition, impairment in working memory and motor tasks, brain and spinal cord axonal degeneration and hippocampal CA1 cell loss [62,63]. The Tg2576 model carries the Swedish mutation in a human APP under the PrP promoter [64]. These mice develop Aβ plaques and show spatial and working memory impairments when tested in the Y-maze and the Morris water maze at 9 months of age [64]. Additionally, synaptic plasticity is selectively impaired as LTP recordings in the Schaffer collateral pathway, but not the mossy fiber pathway, was completely abolished [65] . Transgenic 5xFAD harbor 3 mutation in the *APP* gene and two in *PS1* gene and accumulate plaques very early in life, typically by 4 to 5 weeks of age [66]. These mice show high neuronal damage and cognitive deficits by 5 months of age [66]. The 5xFAD model is one of the few models showing LC damage and inflammation [67]. However, this is seen at 4.5 months of age, an age that is months after the onset of plaque deposition.

Current models of AD have been very useful tools to investigate the consequences of extensive Abeta plaque deposition and its regulation [13]. For example, they have demonstrated that plaques have a primary role in AD neuronal loss [68]. They have also served to assess potential therapeutic interventions [13]. However, they have yet to recapitulate some major anatomical pathology, and biochemical and behavioral features [13]. Very few *in vivo* studies have investigated the role of noradrenergic mechanisms in APP-related processes [13]. Furthermore, current AD mouse models do not recapitulate early LC degeneration in AD [30]. Specifically, LC neuronal loss or lower NA levels in the brain of genetic AD models have not been shown at pre-plaque stages. LC cell death or damage has been reported only in a few lines and only months after plaque deposition has set in [67,69,70].

1.1.8. Description of the AD model used in this study, APP/PS1 double transgenic mice

A well-established AD mouse model is the double transgenic Mo/HuAPP695Swe/HuPS1-ΔE9 mouse. This line carries mutant variants of APP and PS1 as transgenes. The mouse APP transgene is the 695 amino acid-long transcript variant with a humanized sequence within the Aβ fragment. The APP transgene also carries the Swedish mutation (K594N/M595L), known to increase Aβ production and to cause early-onset AD [71,72]. The PS1 transgene is a human PS1 that lacks exon 9. The splice-site mutation leading to the in-frame skipping of exon 9 is associated with early-onset AD [25] .Bigenic mice overexpress APP and PS1, and develop Aβ plaques by 6 months of age. The expression of each transgene is controlled by a mouse prion protein promoter element. Because the two transgenes co-integrated into the same locus, they co-segregate as a single locus. These mice (from here on only referred to as APP/PS1) were first reported by Jankowsky *et al.* in 2001 [73]. APP/PS1 mice were used in this study and were kindly provided to us by Dr. Stephan Paxian (formerly at the University of Münster, Münster, Germany).

1.1.9. Aim of work, objectives and hypothesis

Transgenic models have been extremely helpful tools and beneficial in the study of AD [60,62]. Although many faithfully recapitulate certain features of AD, such as Aβ plaque deposition, brain inflammation, hyperphosphorylated tau and memory impairments, they fail to mimic others [30]. For example, LC cell loss is not observed in these mice, although its involvement to AD pathology in humans is well established [30,38]. The exact contribution of LC loss to the pathology of AD is yet to be elucidated.

Currently, we rely on chemical or surgical methods to ablate LC neurons in transgenic AD models at pre-plaque stages. N-(2-chloroethyl)-N-ethyl-2-bromobenzylamine (DSP-4) has been established as the preferred noradrenergic neurotoxin to target LC neurons [38,39,74,75,76]. These models have been a useful tool; however their specificity to noradrenergic neurons and the validity of their results (as affected by compensatory mechanisms to surgical lesions) have been questioned [75,76,77]. More refined, novel genetic models mimicking LC loss will allow us to investigate the exact contribution of LC loss to AD pathogenesis and progression of the disease.

We aimed to address this question by generating a new AD model of early stages. We wanted our new model to mimic cognitive impairment, LC neuronal loss and lower brain NA levels, preceding plaque deposition. To that end, we crossed LC-deficient Ear2 (-/-) mice to the well-established APP/PS1 double transgenic model of AD. We confirmed that our new model mimics all features we aimed to recapitulate. This made our model a more suitable one to study the early stages of AD pathogenesis and disease progression. This leads us to suggest that NA is a modifying factor of AD-like pathology.

1.2. Parkinson's Disease

1.2.1. Prevalence of the disease

Parkinson's Disease (PD) is a progressive and chronic neurodegenerative disease associated with motor symptoms [78]. PD affects 1.5% of the global population over 65 years of age [78] and it is the second most prevalent neurodegenerative disorder [2]. In the European Union, more than 500 000 people are estimated to suffer from the disease [2]. Furthermore, no cure exists to date for PD. Currently, only a symptomatic therapy is available. Symptoms can be improved by pharmacotherapy, including levodopa, dopamine receptor agonists or monoamine oxidase B inhibitors, or through surgical strategies, such as deep brain stimulation for patients with severe motor fluctuations [78].

1.2.2. Description of the disease

There are four cardinal symptoms of PD, namely bradykinesia, rest tremor, rigidity and postural instability [79]. Additional PD motor features include loss of automatic movements, such as arm swing, loss of blinking, reptile stare and difficulty to perform two simultaneous motor tasks [79]. It is increasingly recognized that non-motor symptoms are also an integral part of the disease[2]. These include autonomic and cognitive impairments. Among the former disturbances are constipation, hypotension, urinary frequency, impotence and sweating [79]. Among the latter impairments are hallucination, delusion, dementia, behavioral abnormalities, depression, sleep disturbances and loss of smell and pain sensation [78,79].

1.2.3. PD pathology and brain regions affected

Biochemically, PD pathology is characterized by the aggregation of eosinophilic intraneuronal inclusions of various shapes and subcellular locations [2,79]. These are called Lewy bodies and Lewy neurites after their first description in 1912 by the German neurologist Friedrich H. Lewy [80]. Lewy bodies and Lewy neurites consist mainly of fibrillar α-Synuclein [2]. Lewy body inclusions is the pathologic hallmark of PD; while the anatomical hallmark is the relatively selective loss of dopamine (DA) neurons in the substantia nigra (SN) [81].

Neuronal loss and Lewy body formation are also present elsewhere. Additional sites of Lewy body deposition are: LC, pedunculo-pontine nucleus, raphe nucleus, dorsal motor nucleus of the vague nerve, olfactory bulb, parasympathetic and sympathetic post-ganglionic neurons, Meynert nucleus, amygdaloid nucleus and cerebral cortices [79]. Non-motor symptoms of PD are caused by lesions to these nuclei and regions other than the SN [79]. And motor deficits are thought to be the consequence of the predominant degeneration of dopaminergic neurons of the SN [2]. The SN is also affected in all parkinsonian conditions, not only in PD [43]. Parkinsonian conditions include, for example, dementia with Lewy bodies, progressive supranuclear palsy and multiple-system atrophy.

The mesencephalon contains the two major dopaminergic cell groups, cell group A9 (substantia nigra) and cell group A10 (ventral tegmental area) (Fig. 3).

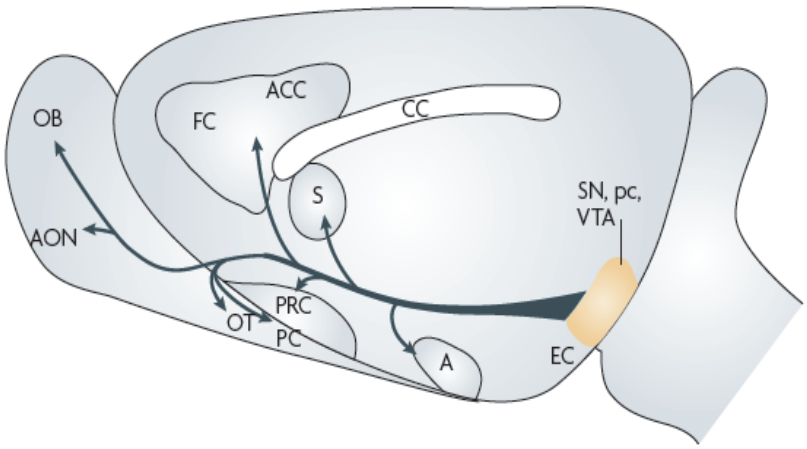

Fig. 3. Schematic representation of the dopaminergic nuclei, substantia nigra and ventral tegmental area and their projections. The substantia nigra (SN, A9) projects to the striatum. The ventral tegmental area (VTA, A10) is the main cortical input of the dopaminergic system, which is limited to the frontal regions, entorhinal cortex (EC) and piriform cortex (PC). Abbreviations: A, amygdala; ACC, anterior cingulate cortex; AON, anterior olfactory nucleus; CC, corpus callosum; FC, frontal cortex; OB, olfactory bulb; OT, olfactory tract; pc, pars compacta; PC, piriform cortex; PRC, perirhinal cortex; S, septum. Modified from Sara, 2009, Nat Rev Neuroscience.

The substantia nigra (SN, cell group A9) encompasses the most ventral part of the entire midbrain tegmentum, just dorsal to the cerebral peduncles [43,82]. Nigral neurons project mainly to the striatum along the nigrostriatal pathway [82]. The SN plays a major role in the control of actions and thoughts and it has been extensively involved in addiction and addictive behavior [50,83,84,85,86].

A10 neurons of the ventral tegmental area (VTA) project mainly to limbic and cortical areas along mesolimbic and mesocortical pathways [82].

1.2.4. Snca gene locus

α-Synuclein (SNCA) is the major structural component of Lewy bodies and Lewy neurites. It is a 14 kDa protein whose primary function has remained elusive, but that is expressed abundantly in presynaptic terminals of regions displaying synaptic plasticity [87,88].

Based on its expression site, on reported SNCA's association to vesicles and on the phenotype of genetic models, SNCA has been proposed to play a role in intracellular trafficking and to regulate synaptic neurotransmission [81,87,88]. However, the exact mechanism is not known.

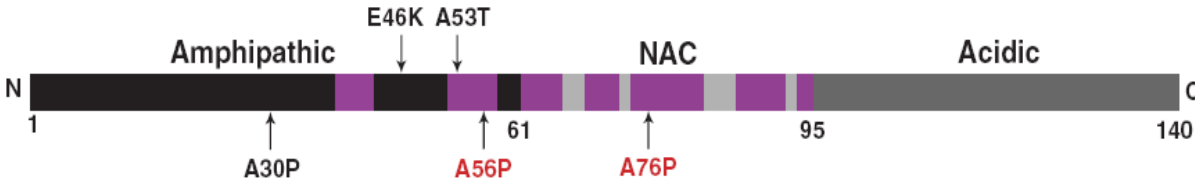

Fig. 4. Schematic representation of the *α-synuclein* gene. Functional domains of SNCA. Mutations known to cause familial early-onset PD are marked in black, while structure-based design mutants are in red. TP-SNCA contains all three substitutions to a proline residue at positions 30, 56 and 76 (below the sequence). Regions involved in β-sheet formation are in purple. The central non-amyloid component (NAC) region is critical for SNCA aggregation. Modified from Karpinar *et. al.*, 2009, EMBO J.

The primary sequence of SNCA is 140 amino acids long and it has been fairly well characterized. Three distinctive regions are present. The amino-terminal, characterized by imperfectly conserved repeats, acquires α-helical structure upon lipid binding, while the carboxy-terminal is highly flexible [89]. The central hydrophobic region, called the non-amyloid component (NAC), is critically involved in SNCA aggregation [88].

SNCA normally exists in an unstructured state [81]. However, it can also form oligomers, protofibrils, fibrils and filaments [90]. Stabilization of these higher-ordered structures may be central to the pathogenesis of PD [81]. Genome-wide association studies identified SNCA as a major risk locus for PD across global populations [91].

1.2.5. Mutations known to cause familial PD

Mutations in SNCA are known to cause familial early-onset PD. The missense mutation A53 was the first to be identified. Two additional mutations have subsequently followed, the A30P in a German kindred and the E46K in a Spanish family [2]. These mutations show an increased propensity for misfolding, and this appears to play a prominent role in cell death [81]. PD-causing mutations also enhance SNCA protofibril formation [88]. In genetic mice models, both the A30P and A53T (singly or in combination) cause increased SNCA inclusions, neurotoxicity and a motor phenotype [92,93]. To date more than a dozen loci and genes have been associated with PD.

Gene dosage has also been associated with PD and multiplications of the wild-type SNCA cause PD. A dose dependency is demonstrated by the earlier age of onset (35 years in average) and high PD prevalence in patients carrying SNCA triplications compared to patients carrying SNCA duplications, who show a more typical late-onset PD phenotype [2]. Likewise, overexpression of human SNCA in mice results in neurophathological and behavioral phenotypes that are proportional to the expression level [94].

A similar scenario as for genetic models of Alzheimer's disease occurred in the PD field. The basis for the creation of numerous genetic mouse models was the identification of mutations known to cause PD. Mutations inherited in an autosomal dominant fashion that are 100% penetrant and that cause the strongest phenotypes have been preferentially used in transgenic models of PD.

1.2.6. Current models of PD

There are many mouse models of PD available to date. Many follow the classical neurotoxin-based approach to selectively ablate dopaminergic cells. Others have been genetically modified to abolish expression of key PD-associated genes. There is also a wide collection of tissue-specific mutants, targeting mainly the dopaminergic system and using one or more of the PD-causing SNCA mutant variants, or the over expression of its wild-type version.

Toxin-based models typically using 6-hydroxydopamine (6-OHDA) or 1-methyl-4-phenyl1-1,2,3,6 tetrahydropyridine (MPTP) target the dopaminergic system [95]. These models have been of great value to understand the consequences of nigrostriatal dopaminergic cell loss and to test symptomatic therapies [96]. However, drawbacks of these models are their considerable limitations for assessing disease-modifying and neuroprotective treatments [78].

Most of the genetically modified mice include knock-outs and transgenics. Among the knock-out lines, SNCA itself and many PD-linked genes (identified as susceptibility genes) have been created. For example, Snca (-/-) mice show reduced rearing activity in the open field, have decreased striatal dopamine levels and a decreased reserve pool of vesicles in the hippocampus [87,94]. None of the genetic models based on PD-linked genes mimic the key symptoms of the disease to their full strength; they show rather a more subtle effect on the dopaminergic system [95]. Dopamine levels in striatum, motor disturbances or abnormal response to dopamine agonists are only slightly altered.

Transgenic SNCA lines, on the other hand, have mimicked more PD-like symptoms. Many single and combinatorial transgenic lines exist to date. Owing to SNCA's prominent role in PD and related synucleinopathies, many SNCA transgenic mice have been created and characterized [for review see [81,93]]. Many new SNCA transgenic mice became available between 2000 and 2005. Most reports included a wt human SNCA and the A53T mutant variant, either alone or in combination with A53T. Promoters used were mainly the murine Thy-1 promoter, mouse or rat Prion Protein (PrP) promoter or rat TH. All transgenic models were based on overexpression. A very broad range of overexpression was detected depending on the promoter used, with the PrP driving a 2.5 to 30-fold expression increase and the Thy-1 promoter an approx. 10-fold

overexpression. Most transgenic mice show SNCA inclusions and some also have lower dopamine levels. A motor phenotype was also present in most of these models.

Although genetic models have more successfully recapitulated some pathological features of PD, such as presence of Lewy bodies or Lewy neurites and motor deficits, they have fallen short in others. For example, cell loss is not always achieved and non-motor symptoms are either absent or not analyzed. To date, no single model created for PD reproduces all key symptoms of the disease [95] and there is a need for more refined animal models [78].

Importantly, genetic models are based on overexpression of a wild-type or mutant variant. This experimental design does not allow for the investigation of the pathology caused by a specific mutation or the mechanism of its toxicity. In overexpresion-based models phenotypes observed can be the result of the particular mutation or the overexpression itself.

1.2.7. Increased toxicity of TP-SNCA soluble oligomers, not fibril-aggregates

Reports in several model systems find no correlation between the rate of fibril and inclusion formation and neurotoxicity [97,98,99,100]. To reconcile these findings, researchers posited that small oligomers of SNCA, rather than fibrils, are the toxic species in PD [101]. Recently, Karpinar *et al.* showed through extensive biophysical analysis and testing in *in-vivo* systems that TP-SNCA has reduced fibrillization propensity [100]. In addition, TP-SNCA forms increased amounts of soluble oligomers, has higher neuronal toxicity and elicits behavioral defects [100]. Through solid-state NMR analysis, aggregates of TP-SNCA and SNCA-A56P have an impaired β-structure formation, showing strong dynamics/disorders. In vivo, TP-SNCA was also shown to be unable to form fibrils in HEK cells, mammalian primary cortical neurons, *C. elegans* and *Drosophila melanogaster* [100]. In the latter two, TP-SNCA impaired dopamine-related behavior, which is relevant and affected also in clinical PD.

1.2.8. Aim of work, objectives and hypothesis

Our objective was two-fold. First, we aimed to fill the need for a more fine-tuned and faithful model to recapitulate Parkinson's disease. Second, we wanted to confirm *in-vivo* in a mammalian system the neurotoxicity of a fibril-deficient Synuclein carrying three Ala->Pro substitutions at positions 30, 56 and 76 (triple-proline substitution SNCA, TP-SNCA). We cloned a targeting vector to generate a knock-in/knock-out conditional TP-SNCA mouse. The new TP-SNCA line will express a floxed-wild-type human SNCA under the endogenous mouse *Snca* promoter. By targeting the start codon, we disrupted the endogenous murine *Snca* and utilized its promoter to drive endogenous levels of expression of the wild-type human SNCA. We created thus, a model not based on overexpression. Upon crossing of our mouse to the DATcre line, progeny will switch to express TP-SNCA in cells of the dopaminergic system exclusively. This will provide an additional level of specificity because the mutant variant of SNCA and its toxic effects will be directed and exclusively restricted to the areas affected in PD patients. In theory, this spatio-temporal and dosage-regulated expression will make our model excel from already existing ones. Following a characterization of the model, our new model will provide a more specific system to investigate the toxicity of TP-SNCA because it is not based on overexpression. We generated the targeting vector, and ES cells were electroporated. So far, successful targeting has been identified in two ES cell clones and blastocyst injection will follow.

Chapter 2. The contribution of noradrenaline to the pathogenesis and disease progression of Alzheimer's disease

2.1. RESULTS

2.1.1. Generation of a new genetic Alzheimer's disease mouse model

In an attempt to better mimic the degeneration of the Locus Coeruleus (LC) and reduction of noradrenaline (NA) levels seen at the early, pre-plaque stage of Alzheimer's disease (AD), we generated a new genetic AD mouse model.

We used mice lacking the *Ear2* gene, which had a reduced LC in a mixed genetic background [59], and we backcrossed these to a pure C57B/6N genetic background for at least 7 generations. C57B/6N Ear2 mutants were then crossed to APP/PS1 mice, a double transgenic AD model expressing mutant versions of APP and PS1. To our knowledge, the Ear 2 (-/-)/APP/PS1 mouse is the first genetic mouse model of AD mimicking the LC reduction at pre-plaque stages of the disease. Current AD models addressing LC reduction depend on chemical or surgical ablation of LC neurons.

2.1.2. Validation of a reduced LC in the new AD model Ear2 (-/-)/APP/PS1

In order to validate the original phenotype of an *Ear2* deletion, namely the reduction of the LC, we analyzed the LC size in the newly generated Ear2 (-/-)/APP/PS1 and in control mice.

This work was carried out partly in collaboration with Inga Urban.

In situ hybridization (ISH) with the LC marker tyrosine hydroxylase (Th) confirmed a reduced LC in Ear2 (-/-) whether or not APP/PS1 were present (Fig. 5). A digoxigenin-labelled Th probe identified the LC nucleus in serial coronal sections of 3-month-old mice (Fig. 5A). Fewer Th(+) cells could be observed in Ear2 (-/-) than in wild-type mice. Cell density was also lower in these animals (Fig. 5A). Sections from APP/PS1 mice were indistinguishable from those of mice not carrying the transgenes. That is, APP/PS1 mice appeared to have as many Th(+) cells as wild-type mice. Analogously, sections from Ear2 (-/-)/APP/PS1 and Ear2 (-/-) mice lacked Th staining to the same extent. Quantification of Th(+) cells demonstrated the drastic reduction of positive Th cells in Ear2(-/-) mice (Fig. 5B). Wild-type mice had an average of 1435.2 (±159.5) Th(+) cells per LC (n=6). The number of Th(+) cells in APP/PS1 mice was slightly reduced, 1255.7 (±70.9) cells per LC (n=6). However, cell numbers were greatly reduced in Ear2 (-/-) mice, whether or not APP/PS1 were present. Respectively, Ear2 (-/-) and Ear2 (-/-)/APP/ PS1 mice had 624.5 (±48.6) and 625.2(±46.4) Th(+) cells per LC (n=6 each genotype). These results were corroborated with a second LC marker, Dbh (Dopamine beta hydroxylase; data not shown).

Overall, Ear2 (-/-) mice showed a 56 % reduction in the number of Th(+) cells. The presence of APP/PS1 had no effect on the number of Th(+) cells detected in the mutant mice.

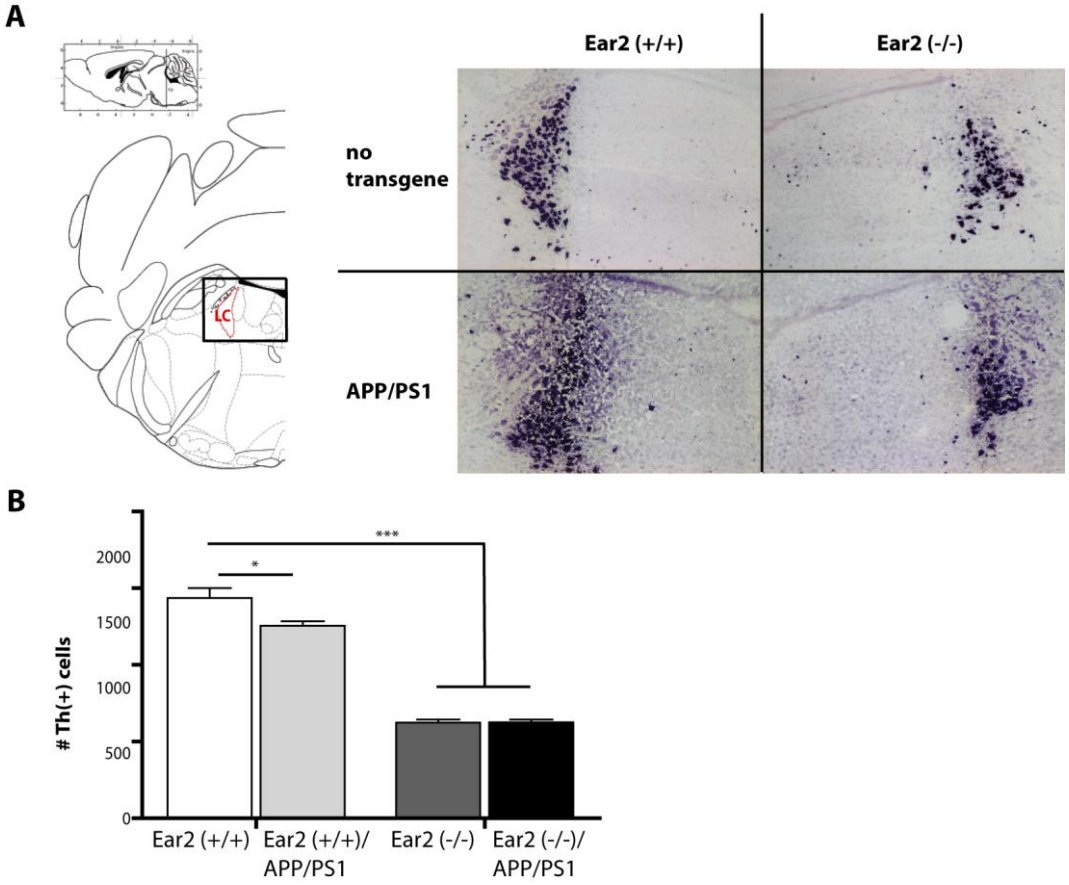

Fig. 5. Validation of a reduced Locus Coeruleus (LC) in the new AD model, Ear2(-/-)/APP/PS1. Ear 2 (-/-) mice had 56% less Th(+) LC cells and APP/PS1 did not drastically affect LC size. **A)** Anatomical location of the LC nucleus in a coronal view. Bregma -5.40mm. Modified from Franklin and Paxinos, 3rd ed. [40]. In-situ hybridization of coronal sections of 3 month old mice. Tyrosine hydroxylase (Th) probe identifies LC cells. Ear2 (-/-) mice showed markedly reduced Th staining compared with Ear2 (+/+) control mice. LC cells from Ear2 (-/-) mice seemed scarcer and less dense. Th staining in APP/PS1 mice resembled that of Ear2 (+/+). **B)** Quantification of Th(+) cells showed a slight decrease in Th(+) cell number in the Ear2 (+/+)/APP/PS1 and a drastic 56% reduction of LC cells in Ear2 (-/-) with or without APP/PS1. *$p < 0.05$; ***$p < 0.001$; n=6 each genotype. Error bars indicate s.e.m.

These data confirmed the reduction of the LC in Ear2 (-/-) in a pure C57B/6N background and in the presence of APP/PS1. Albeit somewhat attenuated, the drastic significant LC reduction detected here is in agreement with the phenotype originally reported by Warnecke et. al. [59].

APP/PS1 mice have slightly less LC neurons, indicating that up to this stage APP/PS1 have no drastic effects on LC size.

2.1.3. Analysis of plaque deposition at 6 months of age

In order to investigate whether chronic NA deficiency, and thus deficiency of NA's anti-inflammatory properties, impacted plaque deposition, we stained Abeta plaques.

Fluorescent microscopy was used to identify Abeta plaques stained with Thioflavin S. Sets of representative sagittal sections throughout the brain of 6-month-old mice were used. Sections from Ear2 (+/+)/APP/PS1 and Ear2 (-/-)/APP/PS1 mice were indistinctive from one another in both the hippocampus and cortex (Fig. 6).

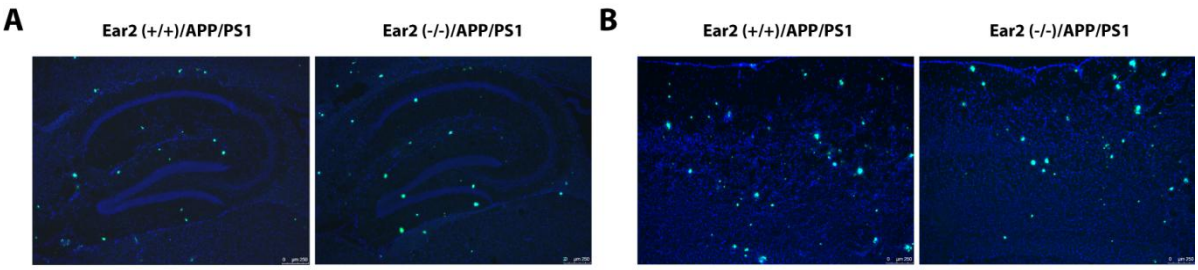

Fig. 6. Thioflavin S staining of Abeta plaques in the hippocampus and cortex. Plaque deposition was the same in the hippocampus and cortex of Ear2 (+/+)/APP/PS1 and Ear2 (-/-)/APP/PS1. Sagittal sections of 6-month-old Ear2 (+/+)/APP/PS1 and Ear2 (-/-)/APP/PS1 were stained with thioflavin S to mark Abeta plaques and subsequently analyzed by fluorescence microscopy. Thioflavin S staining of Abeta plaque in the hippocampus (A) or cortex (B) was the same for both genotypes.

Abeta plaque staining was identical for mice with or without a chronic reduction of NA. Sections from Ear2 (+/+)/APP/PS1 and Ear2 (-/-)/APP/PS1 mice had the same plaque load in both the hippocampus and cortex. Plaque deposition seemed, at least up to 6 months of age, unaffected by the lack of NA.

2.1.4. Quantification of NA levels throughout the brain in young mice

In order to assess whether a reduced LC translated into lower NA levels throughout the brain, we measured NA concentration in the olfactory bulb, hippocampus, frontal cortex and cerebellum. The former three are regions with high LC innervation and are relevant for learning and memory. The cerebellum was included as control because it is less innervated by the LC but it is not implicated in memory.

This work was carried out partly in collaboration with Inga Urban.

HPLC was used to quantify NA concentration in brains of 3-month-old mice (Fig. 7). In the olfactory bulb, NA concentration in wild-type was 0.3586 (±0.026) ng/mg of tissue, while Ear2 (-/-) had only 0.1252 (±0.021) ng/mg of tissue (Fig. 7A). The frontal cortex of wild-type mice contained 0.4636 (0.022) ng/mg of tissue. And NA dropped to 0.219 (±0.052) ng/mg of tissue in the Ear2 (-/-) (Fig. 7B). Similarly, NA concentration in the hippocampus was 0.532 (±0.045) ng/mg of tissue and only 0.16 (±0.036) ng/mg of tissue in Ear2 (+/+) and Ear2 (-/-), respectively (Fig. 7C). A strong reduction of NA was also detected in the cerebellum, where wild-type mice contained 0.5276 (±0.053) ng/mg of tissue and Ear2 (-/-) 0.3597 (±0.028) ng/mg of tissue (Fig. 7D). Throughout the brain, NA levels of APP/PS1 mice were comparable to those of mice not carrying the transgenes (Fig. 7).

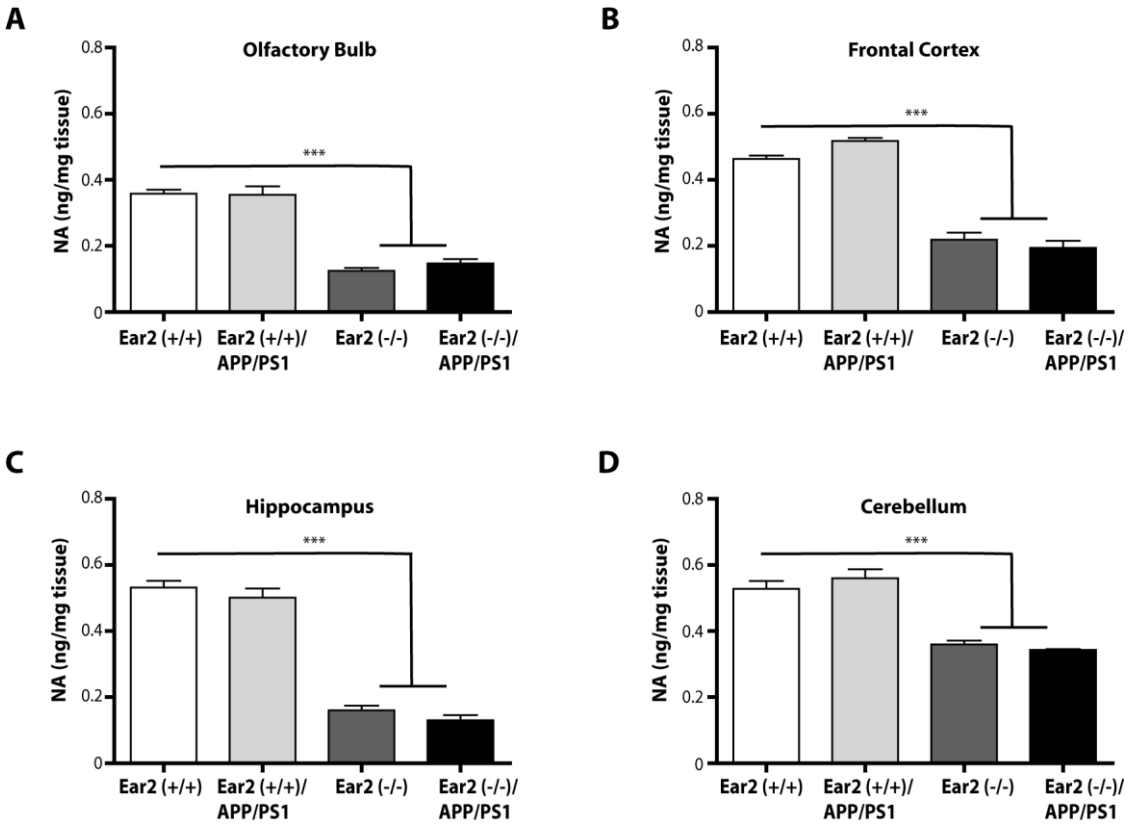

Fig. 7. HPLC quantification of noradrenaline (NA) concentration in the brain. Reduction of the LC resulted in lower noradrenaline levels throughout the brain. Areas with high LC innervations were most affected. A) NA loss in the olfactory bulb of Ear2 (-/-) and Ear2 (-/-)/APP/PS1 mice. Ear2 (-/-) mice showed a 65.1% loss of NA. Mice carrying APP/PS1 had similar levels of NA to those mice negative for the transgenes. **B)** In the frontal cortex, Ear2 (-/-) mice lost 52.8% of NA compared to wild-type mice. The presence of APP/PS1 had no effect on NA concentration. **C)** NA levels in the hippocampus of Ear2 (-/-) mice had a drastic reduction of 70%. APP/PS1 had no impact on NA levels in the hippocampus either. **D)** NA levels in the cerebellum of Ear2 (-/-) mice were reduced by only 31.8%, albeit still extremely significant. APP/PS1 positive or negative mice had comparable levels of NA. Compared to wild-types, the cerebellum of Ear2 (-/-) mice lost about one third of their NA level, whereas all other regions lost more than half. NA levels were affected by Ear2 exclusively and not by APP/PS1. Levels of NA loss correlated with the degree of LC innervation in the respective brain area. Hippocampus, frontal cortex and the olfactory bulbs are regions with high LC innervations and are also relevant for learning and memory. For all brain regions, ***$p < 0.001$; $n \geq 5$ each genotype. Error bars indicate s.e.m.

Although NA reduction was severe in all regions surveyed, the cerebellum of Ear2 (-/-) mice lost a lower proportion of NA. That is, NA in the cerebellum was reduced by 31.8% compared to wild-type mice. However, the olfactory bulb, frontal cortex and hippocampus of Ear2 (-/-) mice lost roughly twice as much NA. They each showed a 65.1%, 52.8% and 70% reduction in their NA levels, respectively.

These data strongly suggest that a reduction of LC cells results in lower NA levels throughout the brain. LC reduction, however, did not seem to affect all brain regions equally. And the degree of NA loss varied greatly among brain regions. While LC cell number was reduced 43.55%, NA loss ranged from 30% in the cerebellum to 70% in the hippocampus. Indeed, the cerebellum is less innervated by the LC. Thus, LC reduction impacts the cerebellum to a lesser extent. On the other hand, LC highly innervates the olfactory bulb, cortex and hippocampus. And, they are highly affected by LC reduction. Importantly, these areas are relevant for learning and memory, which are the first to be affected in AD. This is also in agreement with the original observations in Ear2 (-/-) mice [59]. Agenesis was reported to be preferential to the dorsal division of the LC which projects to cortical areas [59].

2.1.5. Analysis of learning and memory

In order to determine whether the chronic reduction of NA in brain regions relevant for memory had a functional impact, we submitted Ear2 (-/-) mice to a learning paradigm at 4 months of age. To investigate if and how the NA reduction affected cognitive function under an AD-like phenotype, Ear2 (-/-)/APP/PS1 mice were also analyzed.

These experiments were carried out in collaboration with the group of Prof. Dr. Michael Heneka (Neurology Dept., University Clinic, Bonn).

The Morris water maze (MWM) is a test of spatial learning and memory, where mice learn to find a hidden platform using spatial cues as a reference. Results from this test revealed that lower NA

levels or the presence of APP/PS1 transgenes caused a cognitive impairment (Fig. 8). This impairment was exacerbated when both factors were combined. Ear2 (-/-) mice had increased escape latencies and swam longer distances to reach the platform than wild-type mice (Fig. 8). A similar impairment was observed in mice carrying APP/PS1. Memory dysfunction was aggravated in Ear2 (-/-)/APP/PS1 mice and these mice took the longest time and swam the longest distances to reach the platform.

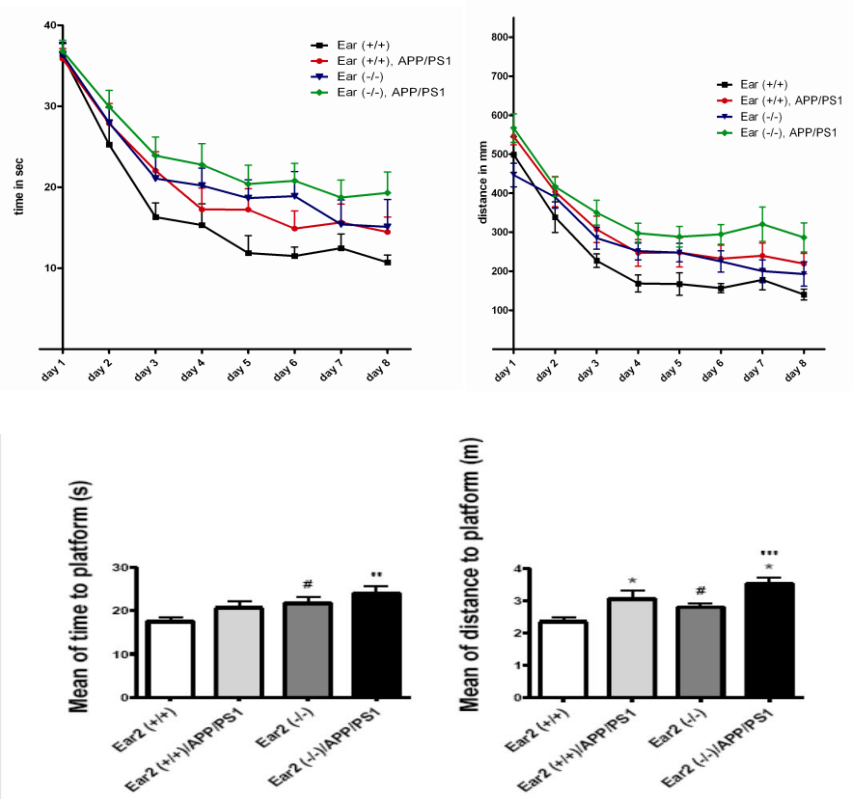

Fig. 8. Morris water maze assessment of spatial learning and memory. Cognitive functions were affected by NA reduction and APP/PS1 transgenes, while these characteristics combined were most detrimental to cognitive performance. Latency and distance to escape to a hidden platform on 8 consecutive days. Bar graphs represent the mean time (s) and distance (m) of each genotype over the complete duration of the experiment. Ear2 (-/-) and APP/PS1 mice showed a mild cognitive impairment compared to wild-type mice. Memory dysfunction was most profound, however, when both Ear2 (-/-) and APP/PS1 were present. *$p \leq 0.05$ (compared to APP/PS1-negative); #$p \leq 0.05$ (compared to wild type); ’’$p \leq 0.01$ (compared to wild type); ’’’$p \leq 0.001$ (compared to wild type); $n \geq 10$ animals per genotype. Error bars indicate s.e.m.

Importantly, we observed that the lack of the neurotransmitter caused a cognitive deficit. The chronic overexpression of the APP/PS1 transgenes also caused a similar impairment, even at this pre-plaque stage. Impaired spatial learning has been reported at 7 months of age [102]. Our data added to this reports showing that a deficiency is already detectable at 4 months of age. If a chronic lack of NA exists in an AD-like background, such as it is the case in Ear2 (-/-)/APP/PS1 mice, cognitive functions seemed most affected. These data indicate that the effects of these factors are synergistic. The scenario in our model, of a chronic NA deficiency and an unbalanced Abeta production vs. clearance, resembles more closely the conditions of a future AD brain. Furthermore, our model is far more specific than previous models addressing LC ablation, typically targeting LC cells surgically or by treatment with the neurotoxin DSP-4.

2.1.6. Confirmation of learning and memory deficiency

To study in greater detail the learning and memory deficits observed in the Morris water maze, we performed electrophysiological recordings on hippocampal slices of 4-month-old mice. Since hippocampal synaptic plasticity is crucial for spatial memory formation, we recorded long term potentiation (LTP) of CA1 neurons.

These experiments were carried out in collaboration with the group of Prof. Dr. Michael Heneka (Neurology Dept., University Clinic, Bonn).

Schaffer collaterals were stimulated and field excitatory post synaptic potentials (fEPSP) were recorded in the pyramidal cell layer. After collecting a stable baseline response for at least 20 min, LTP was induced by theta burst stimulation (4 trains of 10 pulses at 100 Hz, 20 ms apart) (Fig. 9A). Peak slopes of fEPSP recordings were averaged over 5 min. before (baseline) and after LTP induction (Fig. 9A, B). We assessed early and late stages of LTP through responses at 10 min (T1) and 60 min (T2) after induction (Fig. 9C). Responses were normalized to baseline. Ear2 (-/-) and Ear2 (+/+)/APP/PS1 mice showed a modest but significant reduction at both early and late stages of LTP (T1 and T2) when compared to wild-type mice. However, slices from Ear2 (-/-)/APP/PS1 mice were almost unable to form LTP and the response to induction was minimal (Fig. 9B, C).

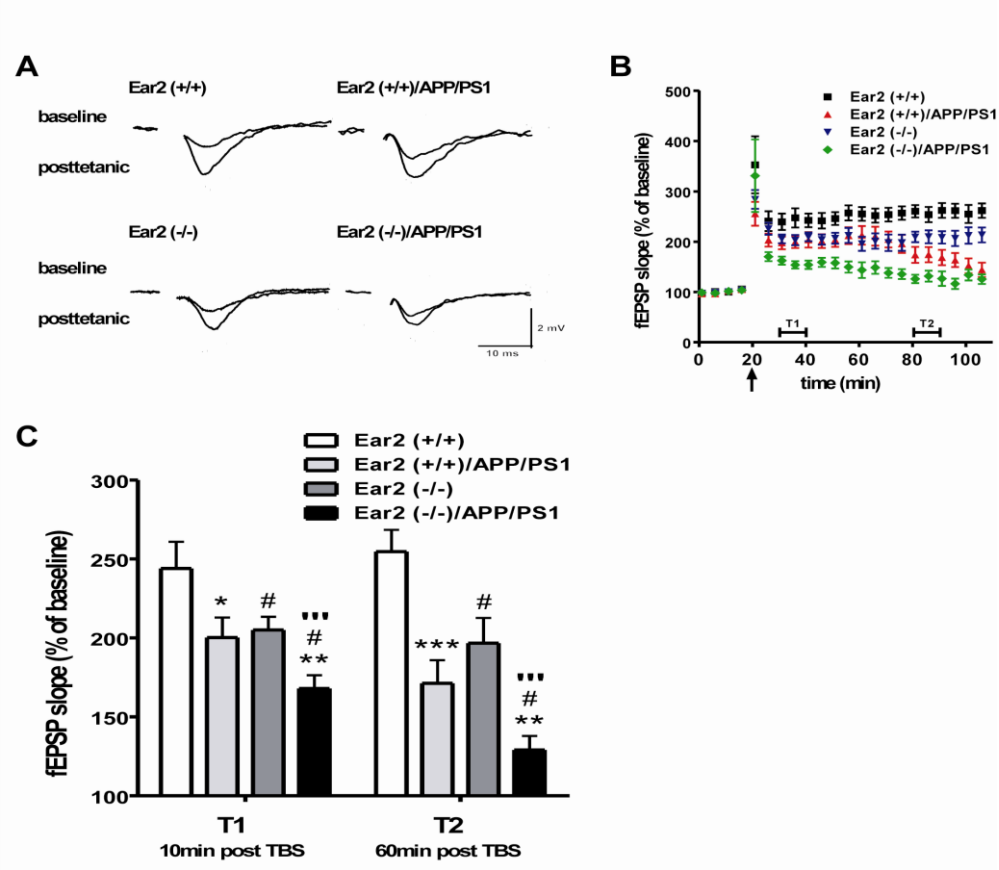

Fig. 9. Electrophysiological recordings in sagittal brain slices of 4-month-old mice. Long term potentiation in hippocampal CA1 was impaired in Ear2 (-/-) and in Ear2 (+/+)/APP/PS1 mice. Impairment was most aggravated in Ear2 (-/-)/APP/PS1 mice and their ability to form LTP was nearly absent. A) Representative responses to long term potentiation recorded in the pyramidal cell layer of the CA1 region. Induced potentials in Ear2 (-/-) and Ear2 (+/+)/APP/PS1 after tetanic stimulation seemed smaller than in wild-type mice. Ear2 (-/-)/APP/PS1 seemed almost unresponsive to tetanic stimulation. **B)** Extracellular field excitatory postsynaptic potential (fEPSP) slope as percentage of baseline obtained before and after LTP induction. Early and late stages of LTP were analyzed 10 (T1) and 60 min (T2) after induction. Ear2 (-/-) and Ear2 (+/+)/APP/PS1 were indeed impaired in both phases of LTP (T1 and T2). Ear2 (-/-)/APP /PS1 had the greatest impairment at both time points. Late stage LTP (T2) was especially affected and fEPSP slope was very similar to baseline. **C)** Quantification of early and late stages of LTP. A very similar early LTP (T1) impairment was observed for Ear2 (-/-) and Ear2 (+/+)/APP/PS1 mice. Impairment was moderate but significant. Early LTP impairment was most aggravated in Ear2 (-/-)/APP/PS1. Early LTP impairment in Ear2 (-/-) and Ear2 (+/+)/APP/PS1 became more pronounced in T2. Late LTP impairment was most aggravated in Ear2 (-/-)/APP/PS1; they were almost unable to form LTP. Factors were additive without interaction shown by two-way ANOVA. Student's t-test: wild type vs. Ear2 (+/+)/APP/PS1 *$p \leq 0.05$ for T1, ***$p \leq 0.001$ for T2; wild type vs. Ear2 (-/-) #$p \leq 0.05$ for T1 and T2; Ear2 (-/-) vs. Ear2 (-/-)/APP/PS1 **$p \leq 0.01$ for T1 and T2; Ear2 (+/+)/APP/PS1 vs. Ear2 (-/-)/APP/PS1 #$p \leq 0.05$ for T1 and T2; Ear2 (+/+) vs. Ear2 (-/-)/APP/PS1 '''$p \leq 0.001$ for T1 and T2; $n \geq 5$ animals per group. Error bars indicate s.e.m.

To assure that LTP impairment could not be attributed to alterations in transmitter release from presynaptic terminals, we assessed paired pulse facilitation (PPF).

Paired pulse facilitation refers to the higher (facilitated) post synaptic response to the second pulse, when 2 pulses (paired) are evoked presynaptically within a very short time (milliseconds apart). Facilitation occurs exclusively at the presynaptic terminal, from where neurotransmitter is released. Facilitation is thought of as the result of an increased probability of vesicular release of neurotransmitter. Thus, changes in PPF would report a change in transmitter release from pre-synaptic terminals. PPF represents short-term presynaptic plasticity.

Comparison of PPF recorded in CA1 with various interstimulus intervals revealed no changes for any of the genotypes (Fig. 10). Transmitter release seemed to be unaffected and thus not the cause of LTP impairment.

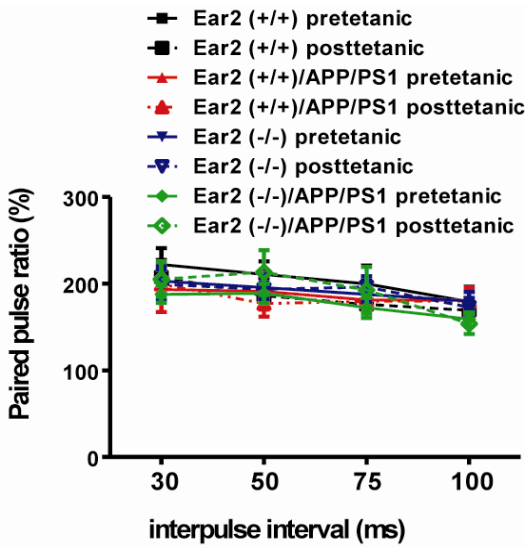

Fig. 10. Paired pulse facilitation before and after LTP induction. Short term synaptic plasticity was unaffected by NA reduction. Paired pulse ratio was similar in all genotypes for all interstimulus intervals recorded (30, 50, 75 and 100ms). Furthermore, PPF was not altered by LTP induction; ratio of PPF was the same before and after tetanic stimulation. $n \geq 5$ animals per group. Error bars indicate s.e.m.

LTP deficits were not associated to deficits in short-term plasticity as indicated by an unaltered PPF ratio. These data indicate that neither the chronic reduction of NA, nor the overexpression of APP/PS1, nor the combination of these two factors has an effect on short-term synaptic plasticity.

Furthermore, the ratio of PPF was unchanged before or after LTP induction (Fig. 10). These data suggest that the presynaptic terminal is unaffected and thus LTP impairment arises from the post-synaptic end.

2.1.7. Rescue of memory impairment

To prove that cognitive deficits seen in our new mouse model were NA specific, we supplied the NA-deficient brains with the NA precursor L-threo-DOPS.

These experiments were carried out in collaboration with the group of Prof. Dr. Michael Heneka (Neurology Dept., University Clinic, Bonn).

L-threo-3,4-dihydroxyphenylserine (DOPS) was i.p. injected together with benserazide, an inhibitor of aromatic acid decarbosylase (AADC) in the periphery, to restore NA levels exclusively in the brain. AADC is needed for the conversion of DOPS to NA. Benserazide inhibits AADC and is unable to cross the brain-blood-barrier. Thus, co-injection of DOPS and benserazide restores NA in the brain exclusively and not in the periphery [74]. NA made in the adrenal gland supplies the periphery and i.p. injection of a NA would interfere with our test by increasing the heart rate and causing hyperactivity. Mice were treated daily with DOPS and analyzed in the MWM 5 hours later, when cerebral NA levels were shown to peak in Dbh (-/-) mice [74].

DOPS treatment partially rescued spatial learning and memory deficits in Ear2 (-/-)/APP/PS1 mice. DOPS-injected Ear2 (-/-)/APP/PS1 mice found the hidden platform significantly faster than vehicle-treated controls (Fig. 11). Two-way ANOVA with repeated measures revealed a significant effect

of DOPS for time ($F_{(1,45)}$ = 4.53, p ≤ 0.5) but not for distance. However, DOPS-treated Ear2 (-/-)/APP /PS1 mice swam significantly less distances from days 5 to 8 than vehicle-treated controls (Student's t-test for days 5 to 8, p ≤ 0.05).

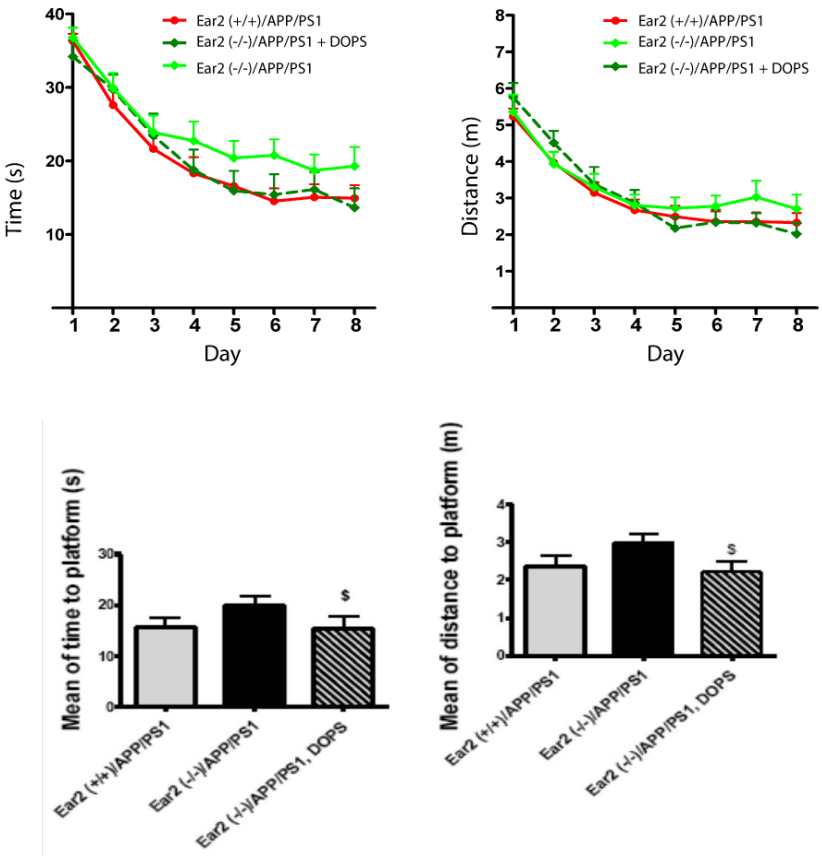

Fig. 11. Morris water maze assessment of spatial learning and memory after acute restoration of NA in the brain. Treatment with the NA precursor L-threo-DOPS restored cognitive deficits arising from a genetic NA depletion. Four-month-old mice received daily i.p. treatments of DOPS and benserazide, an inhibitor of aromatic acid decarboxylase (AADC). AADC converts DOPS to NA. Because benserazide is unable to cross the brain-blood-barrier, co-injection restores NA exclusively in the brain and not the periphery. DOPS-treated Ear2 (-/-)/APP/PS1 mice performed significantly better in the MWM compared to vehicle-treated mice (injected with vehicle solution). Performance of treated mice was comparable to that of Ear2 (+/+)/APP/PS1, suggesting that at least the contribution of a reduced LC to the cognitive impairment can be alleviated by acute NA supplementation. Student's t-test over all days: Ear2 (-/-)/APP/PS1 vs. Ear2 (-/-)/APP/PS1 + DOPS $^{\$}p \leq 0.05$; $n \geq 14$ animals per group. Error bars indicate s.e.m.

Acute NA restoration partially rescued the spatial memory impairment caused by a genetic NA deficiency even under an AD-like background. In the Ear2 (-/-)/APP/PS1 mice, DOPS treatment brought performance in the MWM to a comparable level to Ear2 (+/+)/APP/PS1 mice. These data suggest that, at least in part, cognitive deficits seen in our model are caused by the lack of NA specifically. Furthermore, these data suggest that at least the NA deficiency component of cognitive impairment in an early AD-like environment can be rescued by acute NA reinstatement.

2.1.8. Analysis of LC size in aged mice

In order to analyze long-term effects of NA deficiency, we analyzed the LC nucleus in 1-year-old mice.

In situ hybridization (ISH) with Th marks LC cells (Fig. 12A). As expected, considerably less Th signal could be observed in aged Ear2 (-/-) mice. The presence of APP/PS1 did not seem to affect LC size and Th signal was similar in sections of APP/PS1 positive and negative mice. Quantification of Th(+) cells revealed a moderate 9.16% reduction of Th(+) cells in aged Ear2 (+/+)/APP/PS1 mice (Fig. 12B). Aged wild type mice had an average of 1284.8 (±127.8) Th(+) cells per LC, while aged Ear2 (+/+)/APP/PS1 mice had 1167.1 (±69.6) cells per LC. Th(+) cell number was markedly less in Ear 2 (-/-) mice, regardless of APP/PS1. Aged Ear2 (-/-) and aged Ear2 (-/-)/APP/PS1 mice had 542.1 (±97) and 553.9 (±86.9) Th(+) cells per LC, respectively.

Comparison of the number of Th(+) cells in 3-month and 1-year-old mice showed that the NA producing nucleus remained for the most part intact through aging (Fig. 12C). Surprisingly, only wild-type mice seemed to have fewer Th(+) cells. The number of LC cells remained constant throughout for all other genotypes.

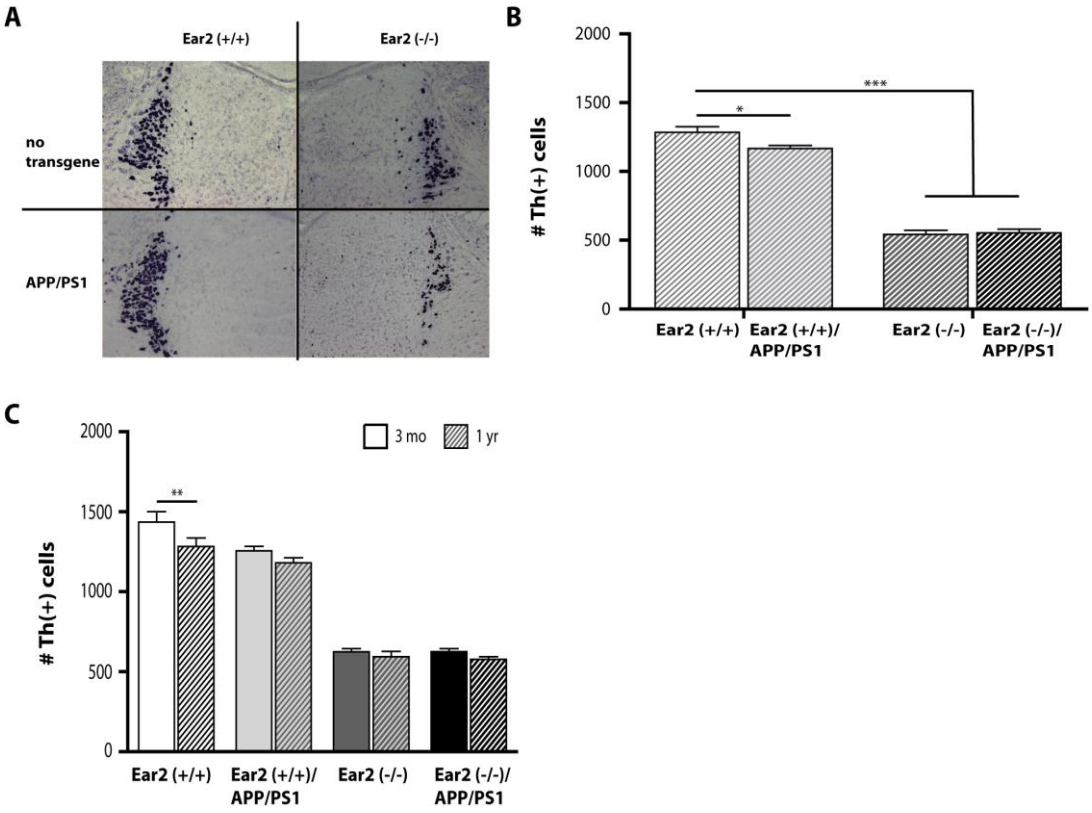

Fig. 12. LC size in 1-year-old mice and comparison to 3-month-old mice. LC cells of aged APP/PS1 mice seemed to be slightly less than in aged wild-type mice. The loss of Th(+) LC cells in Ear2 (-/-) with or without APP/PS1 was extremely significant. Comparison of LC cell number in young and aged revealed that for the most part the nucleus remained intact. Th marks LC cells. **A)** *In situ* hybridization of coronal sections of 1-year-old mice. Ear2 (-/-) mice with or without APP/PS1 showed markedly reduced Th staining compared to wild-type controls. **B)** Quantification of Th(+) cells showed a 57.8% reduction of LC cells in aged Ear2 (-/-). Aged Ear2 (+/+)/APP/PS1 had a modest, yet significant, reduction of Th(+) cells compared to aged wild-types. **C)** Comparison of Th(+) LC cells in 3-months and 1-year-old mice. Interestingly, the only difference was seen in wild-type mice. Otherwise, the nucleus remained intact and Th(+) cell numbers were very similar in young and aged mice of the same genotype. *p< 0.05; **p < 0.01; ***p < 0.001; n=10 each genotype. Error bars indicate s.e.m.

The decrement of Th(+) neurons in aged Ear2 (-/-) mice represented a 57.8% LC loss. At 1 year of age, APP/PS1 mice continued to have slightly less LC neurons than wild-type mice. Besides, no further LC loss was detected as an effect of aging or the extensive plaque accumulation.

These data indicate that the LC remains intact even after a long-term lack of NA or long-term plaque deposition. Through the aging process, the nucleus seems moderately affected. Whether this is functionally relevant will be addressed in the following experiments.

2.1.9. Effects of aging on NA levels

To analyze whether aging affected NA levels under normal and diseased conditions we quantified NA concentrations in the olfactory bulb, frontal cortex, hippocampus and cerebellum and compared them to those at 3 months of age.

2.1.9.a. HPLC quantification of NA in the brain of aged mice

HPLC was used to quantify NA content in learning-relevant regions, with high LC innervations (Fig. 13). We concentrated on the same brain regions as in the young 3-month-old cohort. They are olfactory bulb, frontal cortex, hippocampus and the cerebellum, the later taken as control tissue. NA concentration in the olfactory bulb of aged wild-types was 0.3842 (±0.046) ng/mg of tissue, while Ear2 (-/-) only had 0.0907 (±0.011) ng/mg of tissue (Fig. 13A). The frontal cortex of wild type mice contained 0.4672 (±0.013) ng/mg of tissue. And NA dropped to 0.1872 (±0.012) ng/mg of tissue in the Ear2 (-/-) (Fig. 13B). Similarly, NA concentration in the aged hippocampus was 0.4573 (±0.055) ng/mg of tissue and only 0.1144 (±0.012) ng/mg of tissue in wild-type and Ear2 (-/-), respectively (Fig. 13C). NA content in the cerebellum of aged wild-type mice was 0.5029 (±0.074) ng/mg of tissue and in Ear2 (-/-) 0.2485 (±0.034) ng/mg of tissue (Fig. 13D).

NA content in aged mice carrying APP/PS1 was only significantly lower in the olfactory bulb and frontal cortex as compared to wild-type mice (Fig. 13A, B). NA concentration in the olfactory bulb was 0.2796 (±0.055) ng/mg of tissue in aged APP/PS1 mice, while in the frontal cortex was 0.3534 (±0.037) ng/mg of tissue. These values represented a 27.2 and 24.4% reduction, respectively.

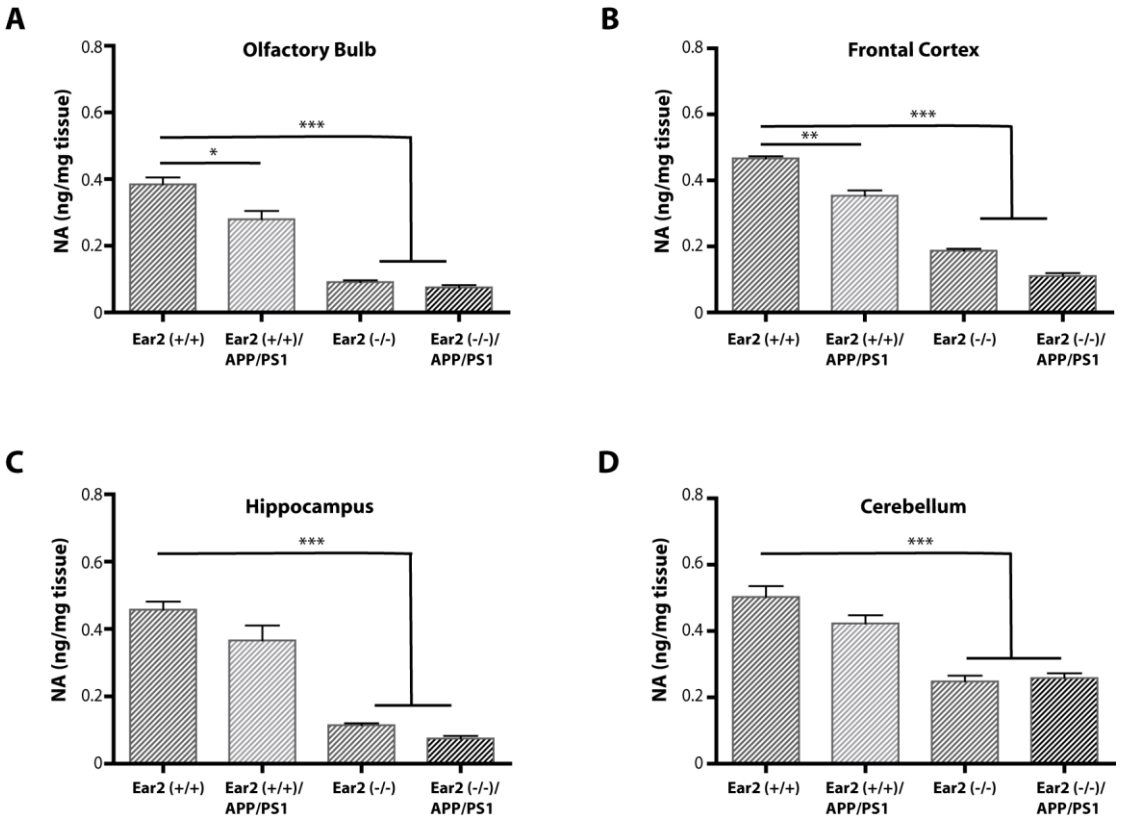

Fig. 13. HPLC quantification of noradrenaline concentration in the brain of 1-year-old mice. Areas relevant to learning and memory and with high LC innervations had the greatest NA loss. A) NA loss in the olfactory bulb of 1-year-old Ear2 (-/-) and Ear2 (-/-)/APP/PS1 mice. Ear2 (-/-) mice showed a 76.4% loss of NA, while APP/PS1 lost 27.2%. **B)** In the frontal cortex, 1-year-old Ear2 (-/-) mice lost 59.9% NA and APP/PS1 mice loss 24.4% NA compared to wild-type mice. **C)** NA levels in the hippocampus of aged Ear2 (-/-) mice had a reduction of 75%. APP/PS1 had no significant impact on NA levels. **D)** NA reduction in the cerebellum of 1-year-old Ear2 (-/-) was 50.6% compared to wild-types. For all brain regions, *$p< 0.05$; **$p < 0.01$; ***$p < 0.001$; $n \geq 5$ each genotype. Error bars indicate s.e.m.

Compared to wild-type, aged Ear2 (-/-) mice lost 76, 60 and 75% NA in olfactory bulb, cortex and hippocampus, respectively. These losses were higher than in young mice. For example, in the olfactory bulb, young Ear2 (-/-) mice lost 65% and aged 76%. In the frontal cortex, NA deficiency went from 53 to 60%, while in the hippocampus from 70 to 75%. The 32% NA loss in the

cerebellum of 3-month-old Ear2 (-/-) reached 51% by 1 year of age. These data indicate that a chronic NA deficiency seems to be accentuated with aging.

2.1.9.b. Comparison of NA content in young vs. aged mice cohorts

Next, we compared NA concentration in young and aged mice to see whether aging affected NA levels throughout the brain under a wild type and disease environments.

In wild-type mice, NA levels remained constant through aging in all brain regions probed (Fig. 14A). From 3 months to 1 year of age, APP/PS1 mice lost 21.2% NA in the olfactory bulb, 31.7% in the frontal cortex, 26.9% in the hippocampus and 35.4% NA in the cerebellum (Fig. 14B). NA loss over time for Ear2 (-/-) mice was also around 25% (Fig. 14C). Aged Ear2-deficient mice lost 27.5, 14.5, 28.5 and 21.9% NA in the olfactory bulb, frontal cortex, hippocampus and cerebellum, respectively. Although NA loss was only significant in the cerebellum, NA values for the other regions were probably too small to reach significance. Ear2 (-/-)/APP/PS1 mice had the greatest NA loss (approx. 45%) for all brain regions surveyed, except for the cerebellum (Fig. 14D). NA loss in the olfactory bulb was 48.9%, in the frontal cortex 43.2% and in the hippocampus 42.3%. Although still extremely significant, NA loss in the cerebellum was only 27.1%.

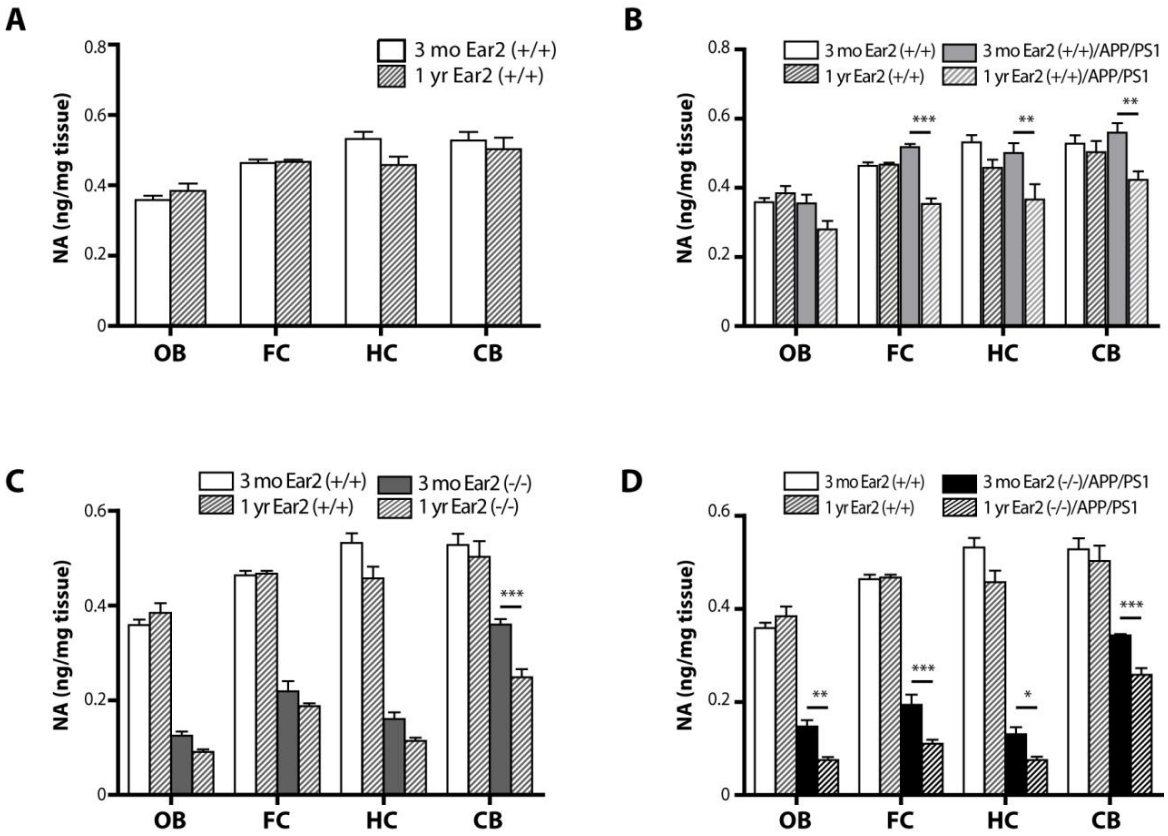

Fig. 14. Comparison of NA levels through aging. Chronic NA deficiency was most accentuated over time under an AD-like background. A) NA concentration in 3-month and 1-year-old wild-type mice. NA levels remained constant throughout aging in all brain regions. **B)** NA content in brain regions of 3-month and 1-year old Ear2 (+/+)/APP/PS1 mice. Bars of wild-type values (as in A) were included as reference. By 1 year of age, mice carrying APP/PS1 had lost approx. 25% NA. **C)** Aged Ear2 (-/-) also lost 25% NA approx. from 3 to 12 months of age, although no significance was reached. Bars of wild-type values (as in A) were included as reference. **D)** NA content in aged Ear2 (-/-)/APP/PS1, however, dropped to about half from 3 months to 1 year. Bars of wild-type values (as in A) were included as reference. For C and D: Levels of NA in young and aged Ear2 (-/-) with or without APP/PS1 are still extremely significantly lower than in wild types (as shown in figures 3 and 9). **OB**, olfactory bulb; **FC**, frontal cortex; **HC**, hippocampus; **CB**, cerebellum; *p< 0.05; **p < 0.01; ***p < 0.001. Error bars indicate s.e.m.

These data indicate that a) under normal conditions (wild-type) there is no NA loss as an effect of aging in our mice, at least not up to 1 year of age, and that the apparent LC size reduction seen by

ISH is seemingly not reflected in NA levels; b) long-term over expression of APP/PS1 or long-term chronic NA deficiency seemed to deregulate the noradrenergic system to decrease NA in the brain; and c) long-term chronic NA deficiency under a diseased environment, such as in Ear2 (-/-)/ APP/PS1, is most detrimental to the noradrenergic deregulation. This scenario resembles closer that of MCI or early AD because LC degeneration occurs before patients become symptomatic. Considering that the lack of NA created cognitive deficits already at 3 months, it is not difficult to imagine that the impairment in aged Ear2 (-/-)/APP/PS1 would also be incremented over time, mimicking disease progression.

2.2. DISCUSSION

2.2.1. Mouse models of AD and LC loss

Many models of AD exist to date; however, most do not mimic LC loss and we rely on chemical or surgical ablation of LC neurons to study this feature of the disease. Chemical or surgical ablation of LC neurons is invasive and it may cause other effects by off-target disruption of cells or by activating compensatory responses after lesion [75,76,77].

Neuronal loss has been detected in a few transgenic AD models, but this is almost exclusively in the hippocampus and at older ages [61,68,103,104]. Importantly, LC cell death is nonexistent at pre-plaque stages in transgenic mice [60]. LC cell loss has previously been reported in the APP/PS1 model used in this study only well after plaque deposition has begun [70]. This is not the clinical scenario. Degeneration of LC neurons occurs very early in AD, presumably even before AD-like symptoms manifest [29,33]. The Ear2 (-/-)/APP/PS1 model has a reduced LC, concomitant reduced NA levels throughout the brain and an enhanced cognitive impairment compared to APP/PS1 mice. Albeit with a NA reduction from embryonic stages, the Ear2 (-/-) mice develop properly and no other overt developmental deficiency was detected [59]. The chronic lack of proper NA levels well before the onset of plaque deposition combined with a well-established AD-like background yields a better approximation to the clinical scenario seen in human patients. We therefore propose the Ear2 (-/-)/APP/PS1 to be a better mouse model for the study of early LC loss and the contribution of chronic NA deficiency to the progression of AD.

2.2.2. Functional consequences of Ear2 knock out and AD

While the developmental anatomical consequences of lacking Ear2 are having a locally reduced LC, the functional consequences extend throughout the brain. First, lower NA levels are found throughout the brain, especially in those regions with high LC innervations. These regions are also important in memory. This is in agreement with published literature reporting lower NA levels in LC projecting regions upon LC neuronal loss [4,31,32,35]. Second, learning and memory are impaired. Our data show that chronic lack of NA in the brain causes learning and memory deficits. These deficits seem greater in the memory consolidation phase, days 4 to 8 of the Morris water

maze (MWM) than in the acquisition phase (days 1 to 4) (Fig. 8). Published data have also implicated NA in memory consolidation [49,105]. More importantly, these results are validated by another NA-deficient mouse model, the Dbh (-/-) [106], where consolidation rather than acquisition was affected. NA deficiency in the Ear2 mutant mice has a genetic basis and they do not undergo invasive procedures nor do they receive toxic treatments before studies are performed. Our data can better establish that it was indeed the lack of NA what caused the cognitive impairments observed.

Alone, APP/PS1 seemed to have a detrimental effect on learning and memory in an NA-independent fashion. The cognitive impairment seen in these mice in the MWM and LTP recordings could not be associated to NA because NA levels in these mice were comparable to those of wild-type mice and re-supplying the brain with NA in Ear2 (-/-)/APP/PS1 rescued only the contribution of Ear2 (-/-) to cognitive impairment. Yet, when APP/PS1 were combined with NA deficiency, cognitive impairments were exacerbated. The combination of chronically lacking proper NA levels with an AD-like diseased environment seems most detrimental to cognitive performance compared to having each one of these characteristics alone. Results from the MWM test and from LTP recordings showed Ear2 (-/-)/APP/ PS1 mice as having the worst cognitive impairment (Fig. 8; 9) as compared to all control groups, namely wild-type, Ear2 (-/-) or APP/PS1 mice. These data suggest that NA is associated to the intensity of an AD-like phenotype at a pre-plaque stage. A scenario that is also likely to occur in MCI patients. These results are consistent with published studies reporting a DSP-4-induced impairment in working and reference memory in APP23 transgenic mice [38]. Previous reports have also shown APP/PS1 mice to be impaired in learning, memory, synaptic transmission and LTP [102,107].

2.2.3. Chronic NA deficiency does not facilitate plaque deposition

Owing to their reduced NA levels, Ear2 (-/-) mice also miss the proper NA anti-inflammatory signal in the brain [52]. Plaque loci are also sites of higher inflammation [38,67]. CD11b(+) activated microglia surround plaques in a mechanism that is thought to aid plaque clearance [55]. Furthermore, reduction in LC neurons has been associated with Abeta deposition [38], neurofibrillary tangles [13] and the severity and onset of dementia [34,35]. It would be then likely

that a genetic NA deficiency could facilitate plaque deposition and that Ear2 (-/-)/APP/PS1 mice would have an elevated plaque load. At 6 months of age, this was however not the case. Thioflavin S staining of 6-month-old Ear2 (-/-)/APP/ PS1 brains showed identical plaque deposition when compared to APP/PS1 age-matched controls (Fig. 6). We cannot rule out the possibility that NA deficiency indeed contributes to plaque burden at a later stage. Plaques deposition may also not be directly affected in our system as it is also not the only feature of AD and other molecular features would need to be assessed.

2.2.4. Memory deficits in Ear2 (-/-) are controlled by LC NA

Ear2-deficient mice have a cognitive impairment due to lack of NA from LC neurons and treatment with the NA-agonist, L-Threo DOPS, alleviates the spatial memory and learning deficits seen in the MWM. Although lower NA in the mutant Ear2 mice originates from developmental stages, rescue of cognitive performance by DOPS treatment shows that NA and no other developmental defect affects the cognitive performance of Ear2 (-/-) mice. This finding becomes more relevant if we consider that apart from NA, LC neurons also produce other neuromodulators. Among others, NPY[57], galanin [57], cocaine- and amphetamine-regulated transcript (CART)[58] and BDNF [56] are produced by the LC.

Consistent with our findings in Ear2 (-/-), L-Threo DOPS is able to partially alleviate the cognitive deficits in Ear2 (-/-)/APP/PS1 (Fig. 11). DOPS alleviates the spatial learning and memory impairment in as much as Ear2 (-/-) (or chronic NA deficiency) contributes to the impairment. DOPS ability to only partially rescue cognitive functions suggests that NA deficiency intensifies the AD-like phenotype at stages before the onset of plaque deposits. Although the mechanisms of action of NA deficiency and APP/PS1 overproduction might act independently of each other to produce an AD-like phenotype, NA deficiency certainly aggravated cognitive performance and thereby acted as a modifier for the disease. This is relevant to the treatment of AD pathology because our findings suggest that successful treatment might require a combination of drugs. Our findings speak for NA as a potential therapeutic to partially alleviate an initial cognitive deficit. And our model could be a suitable one to test potential therapeutic compounds or their combination.

2.2.5. NA levels in aged mice

At 1 year of age, regions most innervated by the LC had the greatest NA loss. These findings were not unexpected as this was also the case for 3-month-old mice. Interestingly, however, by 1 year of age APP/PS1 mice showed significantly lower NA levels than their age-matched wild-type controls (Fig. 13), reflecting a greater systemic deregulation after 6 months of plaque accumulation. Lower NA levels, comparable to the ones we report here, have also been reported in older transgenic mouse models of AD [39,67,108]. One-year-old Ear2 (-/-)/APP/PS1 tended to have even lower NA concentration in memory-relevant regions than Ear2 (-/-) (Fig. 13B, C). These data seem to indicate that NA-deficiency is most accentuated in aged mice if under a disease environment.

2.2.6. NA levels through aging in wild-type and diseased conditions

In order to reveal whether NA levels had an aging component, we compared NA content in 3-month and 1-year-old mice. NA content in wild-type mice remained constant through aging. This is contrary to what is reported for humans, where NA decreases with age [44]. We cannot rule out the possibility that NA in wild-type mice could decrease at an older age. Surprisingly, the number of LC cells decreased by 10% from 3 months to 1 year in wild-type mice (Fig. 12C). Because the decrease is not dramatic, there seems not to be an aging component to NA levels in 1-year-old wild-type mice.

The already low NA levels in young Ear2 (-/-) mice dropped to even lower levels with age and we observed and approx. 25% NA decrease in all regions analyzed (Fig. 13C). NA loss was not associated to LC cell loss because the number of Th(+) cells at 3 months and 1 year were the same. Chronic NA deficiency seems to be accentuated with age, suggesting there may be a negative feedback signaling. Surprisingly, Ear2 deficiency deregulates the expression of only a very small set of genes in the hippocampus (microarray data shows 18 up and 5 down regulated genes; unpublished data from Prof. Henneka's lab), indicating only a more local impact. Whether the NA decrease in aged mice is the result of a compensatory regulation of NA over a long-term impaired brain that was already less plastic, or an overall poor signaling circuitry back to the LC, would have to be further investigated.

Ear2 (+/+)/APP/PS1 mice had modestly less LC cells than wild-type mice at 3 months and 1 year of age (Fig. 5B; 12B, C). This is in keeping with published literature reporting a high LC loss in the same APP/PS1 transgenic model at an older age (16 to 23 months) [70]. Taken together, APP/PS1 seemed to have a gradual but steady loss of LC neurons, perhaps facilitated by plaque accumulation. NA levels were similar to wild-type mice at 3 months and lower at 1 year. And through aging, APP/PS1 lost approx. 25% NA. Lower NA levels at post-plaque stages has also been reported for other APP transgenics, such as in the PS:APP [39,108] and 5xFAD TgAPP [67] mice. These data argue for the transgenes to exert a deregulatory effect on the NAergic system perhaps by their long-term overexpression and the accumulated aggregation of Abeta plaques. Accordingly, microarray data (unpublished data from Prof. Henneka's lab) from hippocampus of Ear2 (+/+)/APP/PS1 mice revealed the expression of over 800 genes to be deregulated.

Ear2 (-/-)/APP/PS1 mice lost over time almost twice as much NA as Ear2 (-/-) or APP/PS1 alone, indicating these two factors to act towards aggravating the AD-like symptom, even if through independent mechanisms.

In conclusion, our model recapitulates AD in a more faithful manner. Namely, we observed in our model the LC loss, decreased levels of NA, higher cognitive impairments and an AD-like pathology that was reinforced with age. Thus, we propose our model to be a more suitable one to study early stages of AD and potential therapeutic compounds. Furthermore, we propose NA to be a modifying factor to AD and as such a promising therapeutic to partially alleviate early cognitive deficits.

Chapter 3. Generation of a new genetic mouse model of Parkinson's Disease

3.1. RESULTS

3.1.1. Construct design

Our objective was two-fold. First, we aimed to fill the need for a more fine-tuned and faithful model of Parkinson's disease. Second, we wanted to test *in-vivo* the neurotoxicity of a fibril-deficient Synuclein carrying three Ala->Pro substitutions at positions 30, 56 and 76 (triple-proline, TP-Snca).

Biophysical data have previously shown TP-Snca to produce a Synuclein variant that is less able to form fibrils but have higher amounts of soluble oligomers [100]. In addition, TP-Snca was shown to have impaired aggregation properties but to be more toxic in mammalian neuronal cultures or in lower organisms [100].

The design of our targeting construct was carried out by Dr. Xunlei Zhou. The objective was to create a conditional synuclein knock out/knock in model. Endogenous expression was sought after and we cloned into the endogenous mouse *Snca* locus. Additionally, spatio-temporal regulation of *TP-SNCA* gene expression was achieved by generating a conditional mutant. Expression of TP-SNCA will be exclusively directed to cells of the dopaminergic system utilizing the Cre/*loxP* system.

The targeting vector contained a wild-type human SNCA that was preceded by a genomic intronic sequence containing the endogenous splicing acceptor and flanked by two *loxP* sites (Fig. 15). Next, a splicing acceptor was included to lead the splicing machinery into the TP-Snca cassette immediately following downstream. An alkaline phosphatase cassette was also included as reporter. Finally, we included a neo cassette flanked by FRT sites as a selection marker for homologous recombination.

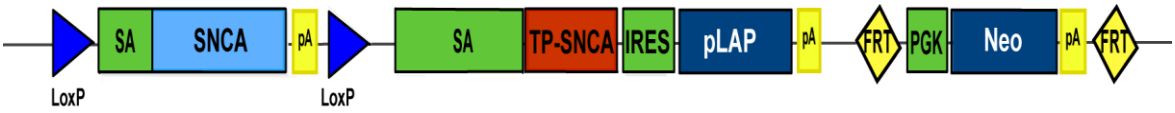

Fig. 15. Schematic representation of construct design. Human wild-type α-synuclein (**SNCA**) was preceded by a short murine genomic intron sequence (containing the endogenous splicing acceptor) and flanked by two *loxP* sites. A splicing acceptor (**SA**) preceded the triple-proline-substituted SNCA (**TP-SNCA**) and an alkaline phosphatase reporter (**pLAP**) cassette. An FRT-flanked neomycin (**Neo**) cassette was included as a selection marker for homologous recombination. Human wild-type SNCA will be produced in these mice. Upon crossing to a DAergic-specific cre-driver line, *e.g.* the dopamine transporter-cre mouse line, dopaminergic neurons of the Substantia Nigra and ventral tegmental area exclusively will switch to produce the TP-SNCA. **pA**, poly A tail; **IRES**, internal ribosome entry sites; **FRT**, flippase recognition target; **PGK**, phosphoglycerate kinase promoter.

3.1.2. Cloning strategy

To be able to work in parallel, our cloning strategy was such that we cloned into a cloning vector from both the 5' and 3' ends of the construct. The cloning strategy was set to pre-assemble 4 different expression cassettes and to subsequently clone them into the cloning vector using restriction enzymes. ET-cloning was also used, first to bring genomic DNA sequence of the Snca locus into the targeting vector, then to clone an additional tetracycline selection cassette and finally to bring our final construct from the cloning into the targeting vector.

This work was carried out in collaboration with Dr. Insa Geffers. All plasmids were kindly provided by Dr. Xunlei Zhou, unless otherwise stated.

3.1.2.a. Preparation of the *pXL112-DTA-genomic SNCA-Tet* vector for cloning of the final construct

3.1.2.a.i. ET cloning of genomic Snca DNA into pXL112-DTA

First, the genomic targeted region of Snca was brought into the *pXL112-DTA* vector from a commercially available BAC clone. We included 5' (5582 bp) and 3' (3298 bp) homologous arms from the targeted region (Fig. 16).

The *pXL112-DTA* vector contained the *Diphtheria toxin A* (DTA) cassette for negative selection of ES cells in which homologous recombination did not occur.

In order to be able to use ET cloning, we first cloned two short homologous sequences of approx. 500 bp each into *pXL112-DTA* using restriction enzymes. We called these H1 and H2.

H1 laid at the 5' end of the 5' homologous arm (Fig. 16). The H1 fragment was first amplified from the BAC clone by PCR reaction. We included restriction sites for *BglII* or *EcoRI* at the 5' end of each the forward and reverse primers, respectively. The 520 bp H1 amplicon was then cloned into the *pXL112-DTA* vector using these restriction enzymes.

Analogously, H2 laid at the 3' end of the 3' homologous arm (Fig. 16). H2 was also PCR amplified from the BAC clone. We included restriction sites for *EcoRI* or *XhoI* at the 5' end of each the forward and reverse primers, respectively. The 517 bp H2 amplicon was then cloned into the *pXL112-DTA* vector using these restriction enzymes to obtain the *pXL112-DTA-H1-H2* vector.

We then used the homologous H1 and H2 sequences to perform ET cloning. We cloned a 9 kb genomic region from the *Snca* gene locus into the *pXL112-DTA-H1-H2* vector (Fig. 16). This vector was termed *pXL112-DTA-genomic SNCA*.

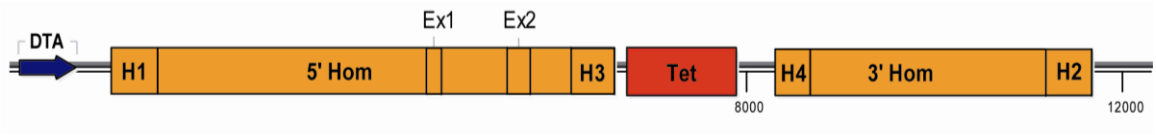

Fig. 16. Preparation of the *pXL-112-DTA-genomic SNCA-Tet* vector. The *pXL112-DTA* vector contained the *Diphtheria toxin A* (DTA) negative selection cassette for homologous recombination in ES cells. ET cloning was used to bring genomic *Snca* sequence from a BAC clone into the *pXL112-DTA* vector using the short homologous sequences H1 and H2. These ca. 500 bp fragments were first PCR-amplified from the BAC clone using primers containing restriction sites at their 5'ends. They were then cloned into the *pXL112-DTA* vector using restriction enzymes. 5' and 3' homologous arms were approx. 5 and 3.5 kb long, respectively. H3 and H4 homologous fragments were used for ET cloning of the final construct into the *pXL112-DTA-genomic SNCA-Tet* vector. H3 and H4 were amplified and cloned in a similar fashion as H1 and H2. Ex1, exon 1; Ex2, exon 2.

3.1.2.a.ii. Preparation of an additional selection cassette, the tetracycline cassette

Analogous to H1 and H2, 2 short homologous sequences flanking the targeted region (endogenous splicing acceptor and 48 bp into exon 3 containing the start codon) were also designed. These H3 and H4 fragments of 490 bp and 399 bp, respectively, were PCR-amplified from the BAC clone. H3 forward primer included a *SfiI* restriction site and H3 reverse primer a *SbfI* at their 5' ends. H4 forward and reverse primers included a *XmaI* and a *SalI* restriction sites, respectively. These PCR products were then sequentially cloned into the *pXL117* vector.

In addition, a tetracycline selection cassette (1647 bp) was cloned between H3 and H4 using the restriction enzymes *XhoI* and *BamHI*. The tet cassette had been previously PCR-amplified with primers containing these restriction sites. This vector was called *pXL117-H3-tet-H4*.

3.1.2.a.iii. ET cloning of the tetracycline cassette into the pXL112-DTA-genomic SNCA vector

Using ET cloning with the short homologous sequences H3 and H4 we brought the tet cassette from *pXL117-H3-tet-H4* into *pXL112-DTA-genomic SNCA*. The tet cassette replaced 250 bp of the targeted sequence in the *pXL112-DTA-genomic SNCA* vector (Fig. 16). The final sequence of DNA fragments in the vector was: *pXL112- H1-5' homologous arm- H3- tet - H4- 3' homologous arm-H2*. However, for practical purposes, this vector was termed *pXL112-DTA-genomic SNCA-tet*.

The purpose of the tet cassette was not only to introduce an additional selection but also to avoid having the 228 bp-long genomic intronic sequence containing the endogenous splicing acceptor and beginning of exon 3, which would be available for homologous recombination (alternative to H3) because they were also included in the final construct. This would result in a missing *loxP* site 5' of SNCA. This was indeed the case in a previous trial and thus this step had to be implemented. This step prepared the vector for cloning of the final construct. Preparation of the final construct is describe in the following section.

3.1.2.b. Preparation of cloning cassettes and assembly of the final construct

The cloning strategy for the final construct involved the pre-assembly of 4 different cloning cassettes (Fig. 17) and their subsequent cloning into the *pXL117-H3* or *pXL117-H4* cloning vectors using restriction enzymes. Cassettes on the 5' end of the construct (Fig. 17, cassettes A and B) were cloned into *pXL117-H3*. Cassettes on the 3' end of the construct (Fig. 17, cassettes C and D) were cloned into *pXL117-H4*. Cloning from both ends of the construct was carried out in parallel and finally the two sides came together by a final step of directional cloning.

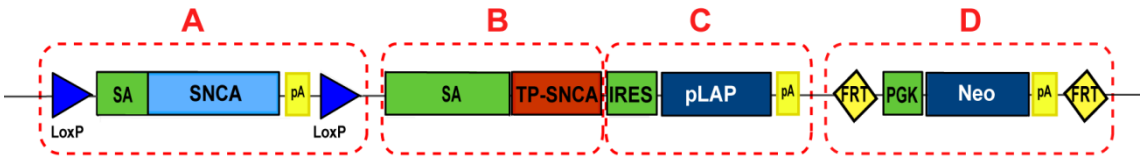

Fig. 17. Preparation of expression cassettes. The cloning vector consisted of four pre-assembled cloning cassettes A - D.

3.1.2.b.i. Assembly of the human SNCA cassette flanked by loxP sites

In order to assure the most faithful endogenous expression of our construct, 202 bp of genomic intron sequence [containing the splicing acceptor (SA)] and 48 bp into exon 3, immediately upstream of the start codon, were included. This cassette had thus 4 components: the *loxP* sites, the intron/exon sequence (250 bp), the SNCA open reading frame (ORF) and a polyA tail. The SNCA ORF and the intron/exon sequence were PCR-amplified and brought together by a 3-step PCR protocol. First, the intron/exon sequence was amplified from the genomic region using a forward primer containing a 5' - *NheI* restriction site and a reverse primer containing at its 5' end 9 bases of homology to the beginning of SNCA ORF. SNCA was similarly amplified from the *pT7-7*-SNCA vector (kindly provided by Prof. Dr. Markus Zweckstetter, Max Planck Institute for Biophysical Chemistry, Gottingen). Attached to the 5' end of the forward primer were 9 bases of homology to the end of the PCR product above (9 last bases of the 48 bp into exon 3). A *BclI* site was attached to the 5' end of the reverse primer. The resulting PCR products (intron/exon sequence, 250 bp and SNCA ORF, 423 bp) were added as templates for a third round of PCR amplification with the forward primer of the intron/exon sequence and the reverse primer of SNCA. Since the two templates had overlapping sequences at the ends, they hybridized generating a PCR product of a fused intron/exon sequence-SNCA fragment (673 bp). This PCR product was then cloned using *NheI* and *BclI* into the *pL452* vector. This vector included a poly A tail and a *loxP* site 5' of the *BclI* site. An additional *loxP* site was conveniently located 3' of the *NheI* site.

The floxed-SNCA cassette (Fig. 17, cassette A) was released from *pL452-SNCA* using *PstI* and *XhoI* and cloned into the *pXL117-H3* vector previously linearized with *SbfI*, which forms compatible ends to *PstI*, and *XhoI*. This formed the *pXL117-H3-floxed-SNCA* vector.

3.1.2.b.ii. Assembly of the triple-proline substitution SNCA (TP-SNCA) cassette with a preceding splicing acceptor (SA)

The strong splicing acceptor sequence from *Engrail2* (En2-SA, 1789 bp) was excised out of *pGT0 Z-AP* using *SalI* and *XbaI* restriction enzymes.

TP-SNCA was PCR-amplified (447 bp) from the *pT7-7-TP-SNCA* vector (kindly provided by Prof. Dr. Markus Zweckstetter, Max Planck Institute for Biophysical Chemistry, Gottingen). The forward primer contained an *XbaI* site and it was followed by the Kozak sequence 5'-C GCC ACC -3'. The reverse primer contained a *SacII* site.

The En2-SA and TP-SNCA cassettes were linked through the *XbaI* site and pre-assembled into the *pGem®-T Easy* system (Promega). This cassette (Fig. 17, cassette B) was then released using *SalI* and *SacII* and cloned into the *pXL117-H3-SNCA* vector, previously linearized with *SalI*-compatible *XhoI* and *SacII*. This step completed the *pXL117-H3-floxed-SNCA-TP-SNCA* vector (Fig. 17, cassettes A and B).

3.1.2.b.iii. Assembly of the selection marker, neomycin cassette flanked by FRT sites

We PCR-amplified the neo cassette and flanking FRT sites using the *pL451 rc* vector as template, a forward primer containing a *KpnI* site and a reverse primer covering the *EcoRV* site present in the plasmid were used. The 1848 bp PCR product (Fig. 17, cassette D) was cloned into *pXL117-H4*, which had been previously linearized with *KpnI* and *EcoRV*.

3.1.2.b.iv. Assembly of the reporter cassette, placental-like alkaline phosphatase (pLAP)

An internal ribosome entry site (IRES) preceded the pLAP and polyA fragment. This cassette (Fig. 17, cassette C) was excised using *EcoRI* from the *pGT0 Z-AP* plasmid. The *EcoRI* 5'-overhangs were excised using the Mung Bean enzyme. The cassette was blunt-end cloned into *pXL117-H4-FRT-Neo* previously linearized with the blunt cutter *SwaI*. Clones with the right orientation were identifed by restriction mapping.

The final step in the preparation of the construct consisted of bringing both ends together. This was accomplished by a final step of directional cloning using *AsiSI* and *SalI* to excise cassettes C, D and H4 from *pXL117-H4-IRES-pLAP-FRT-Neo*. This insert was cloned into the *pXL117-H3-floxed-SNCA-TP-SNCA* vector. The final construct in the cloning vector was: *pXL117-H3-floxed-SNCA-TP-SNCA-IRES-pLAP-FRT-Neo-H4* (Fig. 13, cassettes A to D).

3.1.2.c. Assembly of the targeting vector

A third and final round of ET cloning was performed using the homologous H3 and H4 sequences in order to bring the final construct from the *pXL117* cloning vector (Fig. 17) into the *pXL112-DTA-genomic SNCA-tet* vector (Fig. 16). This step replaced the tet cassette with the cloning cassettes. The resulting vector constituted the targeting vector and it was termed: pXL112-DTA-SNCA to P3-neo.

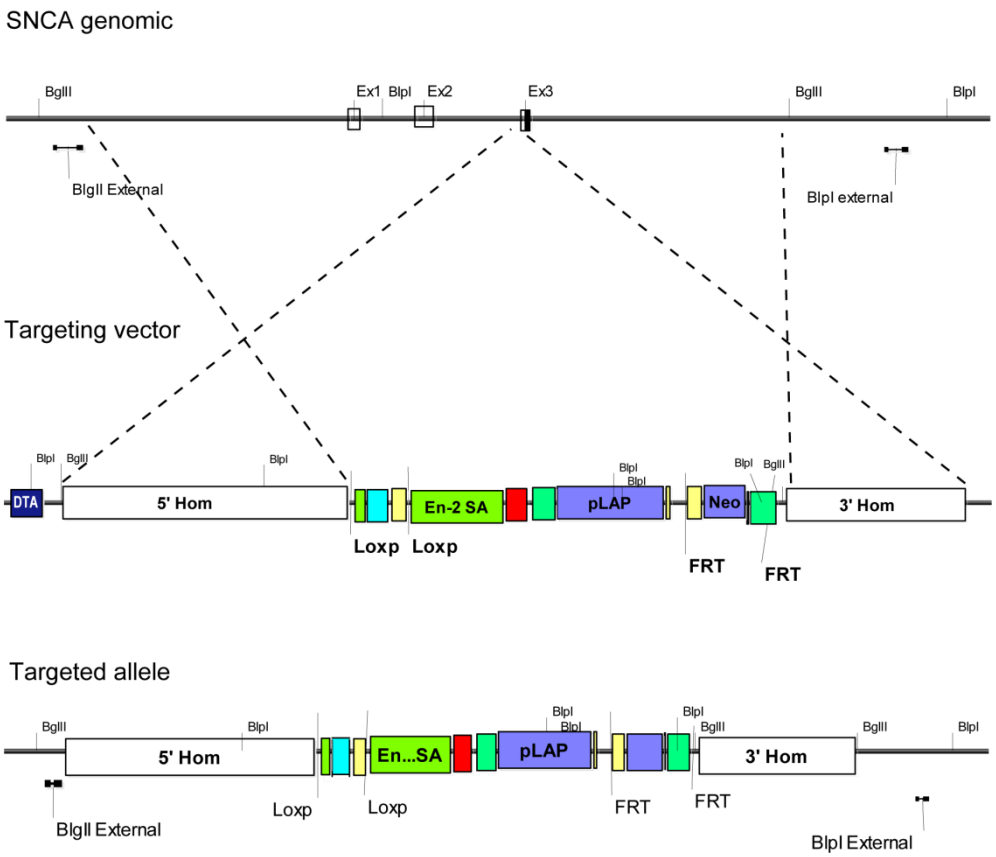

Fig. 18. Targeting vector and targeted allele of Snca.

3.1.3. Electroporation of the targeted vector into ES cells and ES cell selection

The final targeting vector was linearized with *SalI*. Electroporation of the purified DNA into ES cells and selection of ES cells that are resistant to G418 (neomycin analog) was kindly performed by Sharif Mahsur (Transgenic core facility, MPI for Biophysical Chemistry, Gottingen).

3.1.4. Screening of ES cell clones

PCR and Southern blot screening of ES cell clones was performed by Dr. Insa Geffers. Genomic DNA of 238 ES cell clones was pre-screened by PCR. One hundred and seven clones were positive by PCR screening. These were subsequently subjected to Southern blot analysis. So far, 2 correctly

targeted ES cell clones have been identified out of 61 clones screened by Southern blot of *BglII* or *BlpI*-digested ES cell DNA using external probes located 5' and 3' of the homologous arms, respectively (Fig. 19). In the near future, verified ES cell clones will be used for blastocyst injection to generate chimeric mice.

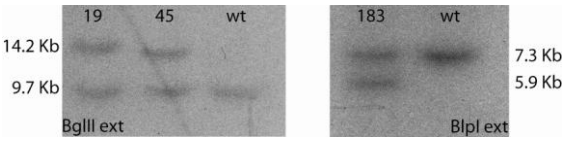

Fig. 19. Southern blotting. *BglII* and *BlpI* external probes were used for Southern blotting to screen for positive clones.

3.2. DISCUSSION

3.2.1. Mouse models of PD

Parkinson's disease was typically modeled by chemical ablation of dopaminergic neurons using neurotoxins specific for the DA system [95] such as MPTP or the pesticide rotenone. Only in the last few decades, genetic models for the disease arose and became available. Not surprisingly, many models target *Snca*, as mutations in this gene are associated to familial PD and Snca is the principal component of Lewy bodies [96]. We have learnt, however, from these models [87,92,94,109,110,111] and from patients [2] that gene-dosage are primordial in the degree of mimicking or manifestation of the disease. Furthermore, genetic mouse models of Snca only partially recapitulate features of PD [94,111]. There is a consensus in the field that better models which more faithfully recapitulate PD are needed [78,81,96]. To that end, we sought to create a model more faithful in the expression level of Snca and in the spatio-temporal restriction of DAergic neurons affected in PD. This model would address *in-vivo* the neurotoxic effects of a synuclein variant that is structurally deficient to form aggregates.

We designed a new model that included three key features of expression and that would separate it from previously existing ones. First, we cloned a floxed human wild-type SNCA into the endogenous *Snca* locus, thereby disrupting the mouse gene. Importantly, using the *Snca* endogenous promoter would ensure endogenous expression levels of the human SNCA variants encoded in our construct. Second, spatio-temporal regulation of expression specifically directed to DAergic neurons would be achieved by crossing our mice to the dopamine transporter-cre driver mouse line [112]. Third, this crossing also serves to drive a switch from wild-type to the mutant variant of synuclein carrying the triple-proline substitution (TP-SNCA). We propose that these features make our model a more refined and better one to study PD, specifically the toxicity of the TP-SNCA. This 2nd generation genetic model will also be useful in the testing and screening of putative therapeutic compounds for the disease.

3.2.2. Validation of the model and investigation of TP-SNCA toxicity

The new TP-SNCA PD model will be crossed to the DAT-cre driver line [112] and a stable colony will be established.

Cre recombinase expression is driven by the DAT promoter and it mediates excision of wild-type SNCA and switching to TP-SNCA approximately at mid-embryonic day 15 [112]. Owing to TP-SNCA's higher toxicity, it would be likely to observe changes driven by its expression in the DAergic system of mice by early adulthood. For example, 3 to 4 month-old mice can be analyzed. This is an age well after all developmental processes have taken place. Mice of this age were also used by Bäckman and colleagues (creators of the DATcre line) to analyze selective deletion of PTEN in DAergic neurons [113] and by the Rubinstein group to analyze DA-D2 receptor ablation in DA neurons using the DATcre line [114]. In our case, behavioral testing will also help us define the age of onset of PD-like symptoms and thereby aid setting an ideal age to perform the molecular analysis.

To prove that TP-SNCA is indeed produced in DAergic neurons, we will perform AP staining on coronal sections of adult mice. Then, histological staining of the brain will analyze its overall cytoarchitecture, especially in the DAergic regions, namely the SNpc and VTA. *In-situ* hybridization with tyrosine hydroxylase [115] will follow to mark and assess intactness of DAergic regions.

DA is transported to the striatum along the nigrostriatal pathway and to limbic and cortical areas (*e.g.* the amygdala and cingulate cortex) along the mesolimbic and mesocortical pathways [82]. DA concentration in these areas will be measured by HPLC. Should TP-SNCA be more toxic, it would indeed follow that these areas be DA-depleted and the mice have motor PD-like symptoms. This rational is in keeping with the clinical scenario observed in PD patients [78].

To validate our model as one for PD, a full battery of behavioral tests will be performed. Tests focusing on motor dysfunction, as that seen in PD patients, will be of special interests. A first quality to be assessed in these mice is posture and gait, which can be detected by careful

observation and footprint patterns[116]. Motor tests such as the rotarod, the balance-beam test, the pulling-wire strength test and the hanging wire grip test will be included [116].

Non-motor PD-like symptoms such as sleep and olfactory disorders are also of great relevance and should be studied [117]. For the former, mice will be placed into home cage running wheels to monitor their locomotor daily activity, preferably also including the complex running wheel with irregularly spaced crossbars [118] to challenge motor control and abilities of the mice. Actograms of activity will reveal whether circadian rhythms or sleep disturbances are present. To test olfactory disorders, an odor habituation test or an odor-based learning paradigm can be used [119].

To analyze the toxicity of TP-SNCA in more depth, we will survey the cellular responses elicited upon its toxic expression. We will perform immunohistochemistry using markers of neurotoxicity. Among others, we will include GFAP, CD11b, nitrotyrosine or the activation of the proteosome/ubiquitin system.

Unfortunately, we still lack a direct detection system that distinguishes *in-vivo* Snca oligomers from fibrils from aggregates. However, structure-based analysis and in-vitro tests in lower organisms like *C. elegans* and *Drosophila* have already shown TP-SNCA's inability to aggregate and its higher toxicity [100]. Our model would now build on those finding in assessing TP-SNCA's toxicity *in-vivo* in a higher organism. These putative neurotoxic effects will certainly be identified and quantified by the methods described above.

In conclusion, our model is not based on overexpression and the expression of the mutant SNCA will be spatio-temporal regulated. These key features make our model a suitable one to study the toxicity of TP-SNCA. We propose our model to be a more fine-tuned and specific model to study PD-like pathology. Additionally, our model will be an appropriate one to assess and validate potential therapeutic compounds.

Finally, the full value of our model relies on its potential to address toxic expression of SNCA in different cell populations. Our conditional floxed mice can be crossed with any cre-driver line to target expression of toxic SNCA to specific cell types or brain regions. For example, crossing our mice to the Th-cre driver line would direct toxic TP-SNCA expression to all catecholaminergic cells, including those of the LC. LC degeneration is also a well established feature of PD [34,43]. Alternatively, our model can be crossed with LC-deficient Ear2 to mimic clinical PD.

Chapter 4. Concluding remarks and future perspectives

The new Ear2 (-/-)/APP/PS1 model of AD recapitulates more AD features. Notably, this model includes LC deficiency, an established early AD feature. This allowed us to study the contribution of LC deficiency to AD pathology. We found NA to be a modifying factor of AD and its deficiency aggravated AD pathology. NA deficiency seems to have a synergistic effect when in combination with APP/PS1; however, the exact mechanism by which NA facilitates AD-like phenotype is yet to be elucidated. To that end, we proved the hippocampal transcriptome of these mice and microarray data are now available. *In situ* hybridization and qPCR of the most deregulated genes will follow to validate microarray results. Follow-up studies seem to indicate that NA deficiency affects components of NMDA receptors and it has a role in the activation of learning-relevant genes. Specifically, we observe in Ear2 (-/-)/APP/PS1 mice a down-regulation of NR2A, an up-regulation of NR2B and the phospho-activation of β-CamKII at Thr286.

It will be interesting to analyze the global inflammation status and activation of the complement pathway in these mice in order to study the consequences of a chronic NA deficiency. Finally, these are a unique model to test potential therapeutic compounds aimed to remedy early features of AD.

The TP-SNCA model will provide the unique opportunity to investigate the contribution of TP-SNCA expression to PD pathology. This model will have spatio-temporal and dose-regulated expression of the toxic SNCA variant and it can be crossed to different cre driver lines to direct specific expression to desired target cell populations. It would be interesting, for example, to survey expression of TP-SNCA in frontal brain regions because damage in PD is preferential, but not restricted to, DAergic neurons. In such a case, a CamKIIcre line can be employed. This is already available in our lab. In addition, LC loss is also an established feature of PD and it would be interesting to cross the new TP-SNCA mice to LC-deficient Ear2 (-/-) mice to investigate the contribution of LC deficiency to PD pathology.

Chapter 5. Materials and Methods

5.1 Animal experiments

5.1.1 Animal housing and breeding

All animal experiments were carried out in compliance with the German Law on Animal Welfare and were approved by the Office for Consumer Protection and Food Safety of the State of Lower Saxony. Mice were housed in transparent, individually ventilated cages (IVCs) with filter tops in specific pathogen free (SPF) conditions. Room temperature and humidity were held constant at 21 °C and 55%, respectively, and animals were kept in a 12 hour light:12 hour dark cycle. Standard chow and water was provided *ad libidium*.

Breeding was established either in pairs or triplets (2 females to one male) and not before the age of 8 weeks. Pups were weaned and ear-marked at the age of 3 weeks at which point 0.5 cm tail biopsies were taken for genotyping. All mice colonies, except for DATcre, were expanded and maintained through regular backcrosses to wild-type (wt) C57B/6N in order to maintain a rich genetic pool. DATcre was backcrossed to wt C57B/6J mice.

Ear2 (-/-) mice were generated by replacing the two first coding exons of the *Ear2* gene by an *IRESLacZ/MC1neo* cassette using the *pKOS/Ear2-39* target vector [59]. The Ear2 mutation was brought into a pure C57B/6N genetic background by backcrossing Ear2 (+/-) mice of a mixed genetic background to wt C57B/6N mice for at least 8 generations before they were crossed to the APP/PS1 mice. Hemizygous double transgenic mice expressing a chimeric mouse/human APP with the Swedish mutation (K670N/M671L) and a mutant human PS1 with Δ exon 9 under the control of the prion protein promoter [120] were maintained on a C57BL/6N background. APP/PS1 mice were crossed to Ear2 KO (Ear2 (-/-)) mice and F1 progeny was interbred. To obtain Ear2 (-/-)/APP/PS1 and all pertinent controls, Ear2 (+/-) parents were mated with only one parent carrying APP/PS1 to ensure all progeny were hemizygous for the transgenes.

5.1.2 Behavioral paradigm – Morris water maze

Mice were single-housed in the testing room under a reversed light/dark cycle (lights off at 8:00 a.m., lights on at 8:00 p.m.) for at least two weeks prior to the beginning of experiments. Tests were performed during the dark phase, when mice are most active. Approximately equal numbers of male and female mice at the age of four months were used, prior to plaque deposition. As no significant differences between sexes were observed, data were combined. Behavior was scored by an observer blind to the genotype and treatment groups**.**

The Morris water maze test was conducted in a pool consisting of a circular tank (diameter 1 m) filled with opacified water at 24°C. The water basin was dimly lit (20-30 lux) and surrounded by a white curtain. The maze was virtually divided into four segments (quadrants). In one of the quadrants, a hidden platform (15 x 15 cm) was present 1.5 cm below the water surface. Mice were trained to find the platform, orientating themselves by means of three intermaze cues placed asymmetrically as spatial references. To prevent strategy learning, they were let into the water in a quasi-random fashion. Mice were allowed to search for the platform for 40 sec. If the mice did not reach the platform in the allotted time, they were placed manually on it. The mice were allowed to stay on the platform for 15 sec before the next trial started. After four trials were completed, mice were dried and placed back into their home cage. Mice received 4 training trials per day for 8 consecutive days. Motion of the mice was recorded by a computerized tracking system that calculated distances swam and latencies (Noldus, The Netherlands). On the ninth day mice were tested for latency to find cued platform.

5.1.3 Administration of drugs and treatment

DOPS was generously provided by Dainippon-Sumitomo Pharmaceutical Company, Ltd. (Osaka, Japan). Ear2 (-/-) and Ear2 (-/-)/APP/PS1 mice were injected with either vehicle or DOPS solution. DOPS solution contained 500 mg/kg, s.c. DOPS, 125 mg/kg, s.c. benserizide, 2 mg/ml ascorbic acid – used to increase DOPS solubility. Benserazide is an inhibitor of the enzyme aromatic L-amino acid decarboxylase (AADC), which converts DOPS to NA. As benserizide cannot cross the blood-brain barrier, DOPS + benserazide treatment restores NA levels to the brain selectively [74,106]. Ear2 (+/+), Ear2 (+/+)/APP/PS1 mice were treated with the corresponding volume of vehicle

solution. Mice were tested in the Morris water maze 5 hr after DOPS injection, when brain NA levels are reported to peak [74].

5.2 Histological methods

5.2.1 Thioflavin S staining of frozen brain sections

OCT-embedded (OCT, Tissue-Tek), fresh frozen 25 µm brain sections were used. Sections were fixed in 4% paraformaldehyde (PFA) for 25 min at room temperature, washed twice in 0.9 % NaCl for 2 min at room temperature and dehydrated through an ethanol gradient. Sections were stored until use at -20° in sealed boxes containing a desiccator bag. Thioflavin S staining was performed as previously described [121,122] with minor modifications. Briefly, sections were thawed and allowed to equilibrate to room temperature for at least 30 min. Sections were pre-washed once briefly in 1x PBS (137 mM NaCl, 2.7 mM KCl, 10 mM Na_2HPO_4, 1.8 mM KH_2PO_4) and then oxidized in 0.3% $KMnO_4$ for 4 min and washed once with water. The bleaching solution consisted of 0.5% $K_2S_2O_5$ and 0.5% oxalic acid. Sections were bleached until the brown color disappeared (approx 15 sec) and washed with water. A reduction treatment followed; this consisted of incubation in 1% $NaBH_4$ solution for 5 min. $NaBH_4$ solution was prepared fresh at least 2 hours before the experiment. Sections were washed 3 times in water and once in 1x PBS. A 0.05% Thioflavin S solution in 50% ethanol was freshly prepared and sections were stained for 8 min in the dark. Sections were differentiated twice in 80% for 10 sec each and rinsed 3 times with plenty of dist. water. A final incubation in a high concentration of phosphate buffer (411 mM NaCl, 8.1 mM KCl, 30 mM Na_2HPO_4, 5.2 mM KH_2PO_4, pH 7.2) was carried out at 4°C for at least 30 min. Sections were briefly rinsed in dist. water and coverslipped using Vectashield Hard Set (Vector) mounting medium containing DAPI. Sections were analyzed using fluorescence microscopy.

5.3 Neurochemical determinations

5.3.1 Noradrenaline quantification by HPLC – electrochemical analysis

Concentration of NA was determined by HPLC with electrochemical detection as previously described with minor modifications [123,124]. Briefly, brains were dissected and washed in ice-cold PBS. Specific brain regions were dissected on ice and immediately flash frozen in dry ice. For HPLC analysis, samples were weighed, homogenized in 100 (olfactory bulb, frontal cortex), 200 (hippocampus, cerebellum) or 300 (brain stem)µl sample buffer (0.1 M perchloric acid, 0.01% EDTA and 0.08 ng/µl 3,4-dihydroxybenzylamine – used as an internal standard) and subjected to two rounds of centrifugation (14 000 x g, 20 min each, 4 °C). Immediately thereafter, 20 µl of the supernatant was injected into a C-18 reverse-phase column (Spherisorb ODS-I 5 µm, 250 x 4.6 mm; Techlab). The isocratic mobile phase consisted of 0.15 M chloroacetic acid, 0.2 mM EDTA, 0.86 mM sodium octyl sulfate, 6% acetonitrile and 2.5% tetrahydrofuran, pH 3. Flow rate was kept at 1.2 ml/min. NA was detected by an electrochemical detector (Coulochem II, model 5200A; esa, Chelmsford, MA, USA) and data was analyzed with the Clarity light software.

5.4 Electrophysiology

Electrophysiological recordings were performed on hippocampal brain slices from 4-month-old mice, obtained following anesthesia with isoflurane (5%) and decapitation. Brains were immediately dissected and sliced sagitally in 400 µm sections using a vibratome (Camden Instruments, Integraslice 7550 PSDS). Hippocampal slices were isolated and maintained at 29°C in an oxygen-enriched atmosphere in artificial cerebrospinal fluid (aCSF) (124 mM NaCl, 4mM KCl, 1.24 mM NaH_2PO_4, 1.3 mM $MgSO_4$, 26 mM $NaHCO_3$, 10 mM D-glucose, and 1 mM $CaCl_2$), for 30 min, followed by incubation in aCSF at elevated $CaCl_2$ (2 mM) for further 30 min. Single slices were moved to an interface-type recording chamber were they remained for additional 15 min. Extracellular field excitatory postsynaptic potentials (fEPSPs) were recorded in the pyramidal cell layer of the cornu ammonis 1 (CA1) region using glass microelectrodes (resistance 0.7 – 2 MΩ) filled with aCSF. The stimulating electrode was placed in the CA2 region within the Schaffer collaterals. Stimuli were applied at constant current, at a duration of 0.1 ms. The initial slope of evoked fEPSPs was measured as an index of synaptic strength. Basal synaptic transmission was assessed by plotting the stimulus intensity (mA) against the peak slope of the evoked fEPSP to generate input-output relations. Paired pulse facilitation (PPF) through two-stimulus protocols

with stimulus intervals of 30, 50, 75 and 100 ms at 30% maximal stimulation intensity. For long term potentiation (LTP) experiments, a 20 min baseline was recorded with an interpulse interval of 1 min at a stimulus intensity that evoked a response of approximately 30% of maximum fEPSP. LTP was induced by a theta burst consisting of 4 trains of 10 pulses at 100 Hz separated by 200 ms.

5.5 Molecular biology methods

5.5.1 Conventional cloning

All conventional cloning was performed using materials from New England Biolabs. High-fidelity enzymes were used when available. All protocols were carried out according to the manufacturer's recommendations. All inserts generated by PCR were sub-cloned first into pGem®-T Easy system (Promega) according to the manufacturer's protocol.

5.5.2 Mini preparations

Mini preparations were performed using the NucleoSpin Extract II (Machery Nagel) and the QIAprep Spin Miniprep (Qiagen) kits.

5.5.3 DNA purification for ES cell electroporation

The sequence-verified *pXL112 DTA SNCA to P3-neo* targeting vector was linearized with the restriction enzyme *SalI*. Digestion efficiency was verified on a test-agarose gel and the linearized vector was phenol-chloroform extracted followed by nucleic-acid precipitation with 2 volumes of ethanol and 1/10 3 M NaAc. After two washes with ice-cold 70% ethanol, the DNA pellet was re-dissolved in sterile 1x TE (10 mM Tris-Cl, 1 mM EDTA, pH 7.6) and kept at 4°C until use.

5.5.4 ES cell electroporation

ES cell electroporation was performed by Sharif Mahsur (transgenic core facility, MPI-BPC). 1 µg linearized vector was electroporated into *129/SvPas* embryonic stem (ES) cells. Clones were screened for integration of the transgene by G418 (Geneticin, neomycin analog) and resistant clones were grown in 24 well plates.

5.5.5 ES cell DNA extraction

To each well, 500 µl lysis buffer (10mM Tris-HCl pH 7.5, 10mM EDTA, 10mM NaCl, 1mg/ml proteinase K, 0.5% SDS) were added and 24-well plates were incubated overnight at 55°C. The following day, the contents of each well were transferred into a 1.5 ml microtube and 200 µl freshly prepared ice-cold NaCl/Ethanol mix (15 µl 5M NaCl per 1 ml cold 100% Ethanol) were added. After inverting several times, samples were centrifuged at 13000 rpm for 15 min at 4°C. The supernatant was discarded. After two washes with 700 µl 70% ethanol, the pellet was briefly allowed to air-dry and re-dissolved in 40 µl TE buffer.

5.5.6 Southern blotting

Overnight digestions (total volume = 50 µl) with BglII or BlpI restriction enzymes were set up and fragments were resolved on a 0.7% agarose gel over several hrs. Upon gel documentation under a UV-lamp, the ladder-containing lane was separated from the gel to avoid unspecific signal given by ladder fragments. The gel was incubated for 15 min in 4x volume of gel (typically 1 Lt) 0.2 N HCl (20 ml conc. HCl in 1 Lt water) with gentle shaking. This step eases the transfer of large DNA fragments to the blotting membrane. Two 20 min-denaturation washes followed in denaturing buffer (0.5 M NaOH, 1.5 M NaCl) with gentle shaking. For blotting, a small piece of Saran wrap was placed on the bench to contain the blotting sandwich. Two pre-cut sheets of Whatman filter paper were pre-wetted in denaturing buffer and carefully overlaid on top of the gel. Upon flipping (to have the gel on top), a pre-wetted in water and pre-equilibrated in denaturing buffer, HybondXL membrane (Amersham) was carefully laid on top avoiding bubbles. Two more pre-wetted in denaturing buffer sheets of Whatman filter paper were place atop and a 10 ml pipette was gently rolled over to assure no bubble were present. Ends of the Saran wrap were folded in as to seal the sandwich to prevent contact from filter papers from the top and bottom. Paper towel

was stacked on top and a small bottle was placed atop to add light weight. DNA blotting was allowed overnight. On the following day, positions of the wells were marked onto the membrane and its upper, right corner was cut for orientation. The membrane was neutralized for 5 min in neutralizing buffer [500 ml NaPi (1 M NaPi, pH 6.7 stock)]. Blotting excess liquid off by placing the membrane in between two Whatman filter papers, the membrane was then UV crosslinked in Stratakinker (autocrosslinking setting, 1200J).

The membrane was then shortly incubated at 65°C in pre-warmed Wash II buffer (1% SDS, 40 mM NaPi, pH 6.7) to equilibrate. 20 ml pre-warmed Church buffer (7% SDS, 300 mM NaPi pH 6.7, 5mM EDTA) were poured into a hybridization tube, the membrane was added and allowed to incubate at 65°C for at least 30 min. Meanwhile radioactive probes were generated from 35 ng PCR templates using the Rediprime™ II DNA Labeling System (GE Healthcare) and ^{32}P labeled dCTPs (Easy Tides Deoxyciytidine 5-triphophate, Perkin Elmer) according the manufacturers' procotols. Primers used to generate PCR templates were: BglII external probe forward primer 5'-AATGCACTCAGTTGAATTATTTC -3' / BglII external probe reverse primer 5'-AATAGCATGGCATATGTGAATAATTC -3'; BlpI external probe forward primer 5'-TCCTGGGAGCAATTTGTTTATAG -3' / BlpI external probe reverse primer 5'-ATTCCTATTCAAACCACCACAAC -3'. Radio-labelled probes were purified using the Illustra™ probequant G-50 micro colums (GE Healthcare) and heat-denatured (99°C, 5 min followed by 5 min on ice). Hybridization was performed at 65°C overnight in 20 ml Church buffer. The following day, the membrane was washed 3x in Wash II buffer at 65°C, sealed in cling film and a Biomax MS film (Kodak) was exposed for several days at -80°C.

5.5.7 ET cloning

Single EL350 were picked from a LB plate (10g trypton, 5 g yeast extract, 10 g NaCl, 15 g agar to 1 liter H_2O) and 1.4 ml LB broth were inoculated and allowed to grow overnight at 32°C at 600 rpm shaking. 1.4 ml LB broth were inoculated with 40 µl of the overnight culture and allowed to grow for 3 hours at 32°C and 600 rpm shaking. Bacteria were made electro-competent by a short centrifugation step of 20 sec at 13 000 rpm at 4°C and 3 washes with ice-cold water. Electro-competent bacteria were re-dissolved in 40 µl ice-cold ddH_2O and 1 µl BAC bMQ-48E8 clones

(Geneservice Ltd.) was electroporated with 1.8 KV. 1 ml LB media was added, the culture was allowed to grow for 1 hr at 30°C with 300 rpm shaking. 50 and 100µl were plated on LB plates containing CAM (25µg/µl) and incubated overnight at 30°C. The following day, 1.4 ml LB with CAM were inoculated with a single clone and incubated overnight at 30°C with 600 rpm shaking. In parallel, vector *pXL112-H1-H2* was digested with *EcoRI* and linearized vector was separated on an agarose gel overnight. The following day, 1 ml of overnight culture was used to inoculate 20 ml of LB broth with CAM and the culture was allowed to grow to an OD ~ 0.5 (2-3 hrs) at 32°C with 230 rpm shaking. During this time, the linearized vector was gel extracted and eluted in 25 µl elution buffer. 10 ml of bacterial culture were transferred into a clean flask and ET-recombinase was induced by heat through a 15-min incubation at 42°C with shaking. The flask was immediately thereafter placed into wet-ice and allowed to incubate for 20 min. Contents were then transferred into a Falcon tube and spun at 5 000 rpm for 6 min at 4°C. Bacterial pellet was re-suspended in 1ml ice-cold water, transferred into a microtube and bacteria were made electro-competent as described above. 100 ng of linearized vector were electroporated and bacteria were allowed to grow. 50 and 100 µl culture were plated on LB with Amp (100 µg/µl) and incubated at 32°C overnight. 10 clones were picked and analyzed via miniprep, PCR and restriction digest.

All other ET cloning steps were carried out in a similar fashion using vectors and inserts as described in the text with appropriate antibiotic selection.

5.5.8 DNA extraction from mouse tail biopsies

Mouse tail biopsies of approx. 0.5 cm were digested overnight in 200 µl PBND buffer (50 mM KCl, 10 mM Tris pH 8.3, 2.5 mM MgCl2, 0.1 mg/ml gelatin, 0.45% v/v NP40, 0.45% v/v Tween 20) plus 3µl Proteinase K (20mg/ml, Roche) at 55°C with 750 rpm shaking. Proteinase K was heat-denatured at 85°C for 1 hr with shaking and tail lysate allowed to cool at room temperature. After a pulse-spin centrifugation, 1 µl of tail extract was used for PCR reaction (Crude tail PCR, modified from[125]).

5.5.9 Genotyping PCRs

A PCR master mix was prepared for individual PCR reactions of 20 µl final volume. Specific primer sequences and PCR product sizes are provided in Table 1. The GoTaq Flexi DNA Polymerase (Promega) was used according to the manufacturer's protocol. Primers were used at a concentration of 5 µM each. For the DATcre line, all 3 primers were added to the master mix and PCR products were analyzed in a 1% agarose gel. The PCR program consisted of an initial denaturing step (94°C) of 3 min, followed by 35 cycles of 94°C - 30 sec, 62°C - 1 min, 72°C – 30 sec. A final elongation step (72°C) of 7 min and a cooling step to 4°C were also programmed. For APP/PS1 either APP or PS1 primers were used in a PCR reaction using only 0.4 or 0.3 µl tail lysate, respectively. PCR conditions were as above except that cycles consisted of 94°C – 1 min, 65°C - 1 min and 72°C – 45 sec. PCR primers detected the transgenes and samples were either positive or negative. PCR products were analyzed in a 1% agarose gel. For the Ear2 line, a 4-primer multiplex PCR reaction was set up and products were resolved on a 2 % agarose gel. PCR conditions were 94°C – 4 min, 35x (94°C – 30 sec, 65°C – 30 sec, 72°C – 40 sec), 72°C – 7 min and 4°C – ever.

Line	Primer name	Primer sequence	Product size
DATcre	IMR6625 com_fo	5'- TGG CTG TTG GTG TAA AGT GG -3'	
	IMR6626 wt_re	5'- GGA CAG GGA CAT GGT TGA CT -3'	wt: 264 bp
	IMRT7997 mut_re	5'- CCA AAA GAC GGC AAT ATG GT -3'	cre: 152 bp
APP/PS1	PSEN1_fo	5'- GGT CCA CTT CGT ATG CTG -3'	
	PSEN1_re	5'- AAA CAA GCC CAA AGG TGA T -3'	PS1: 500 bp
	APP1597	5'- GAC TGA CCA CTC GAC CAG GTT CTG -3'	
	APP1598	5'- CTT GTA AGT TGG ATT CTC ATA TCC G -3'	APP: 350 bp
Ear2	Ear2-nFo2	5'- GAC TCC ATG CAT AGC TGG TAC TTG G -3'	
	Ear2-nRe	5'- AGC ACT TCT TGA GCC GAC AGT ACT G -3'	wt: 380 bp
	LacZ_Fo	5'- CGT CAC ACT ACG TCT GAA CGT CG -3'	
	LacZ_Re	5'- CAG ACG ATT CAT TGG CAC CAT GC -3'	-/-: 400 bp

Table 1. Genotyping primers and product sizes.

5.5.10 Colorimetric in situ hybridization

Automated *in-situ* hybridization procedures followed those described in Yaylaoglu *et al.* 2005 [126,127]. These include tissue collection, sectioning, DNA template production, RNA probe synthesis and *in-situ* hybridization protocols. The following TH-specific (NM_009377) PCR primers were used: forward 5'-GATTGCAGAGATTGCCTTCC- 3' and reverse 5'-CCTGTGGGTGGTACCCTATG-3'. The Agilent's 2100 Bioanalyzer was used for quantification and quality control of RNA probes.

5.6 Statistical analysis

All statistical evaluation was performed using the GraphPad Prism 5 software (San Diego, CA). Values were considered significantly different when $p < 0.05$. Data points and bars represent mean ± SEM in all figures unless otherwise indicated. *$p \leq 0.05$; **$p \leq 0.01$ and *** $p \leq 0.001$. Behavioral data of the MWM test were analyzed by two-way ANOVA with repeated measurements (independent between subjects variables: APP/PS1 transgene, Ear2 (-/-) and DOPS treatment, dependent between subjects variables: latency or distance, independent within subject variable: day). All other experimental data were analyzed by two-way ANOVA if not stated otherwise. Bonferroni multiple comparisons post-tests were used. If a significant effect of the independent variables was found in the ANOVA, Student's t-test for intergroup comparison was performed subsequently.

REFERENCES

1. Price DL, Sisodia SS, Borchelt DR (1998) Genetic Neurodegenerative Diseases: The Human Illness and Transgenic Models. pp. 1079-1083.
2. Gasser T (2009) Molecular pathogenesis of Parkinson disease: insights from genetic studies. Expert Rev Mol Med 11: e22.
3. Alzheimer's_Association (2011) 2011 Alzheimer's disease facts and figures. Alzheimer's & dementia : The Journal of the Alzheimer's Association 7: 208-244.
4. Matthews KL, Chen CP, Esiri MM, Keene J, Minger SL, et al. (2002) Noradrenergic changes, aggressive behavior, and cognition in patients with dementia. Biol Psychiatry 51: 407-416.
5. Alzheimer's DI (2011) How many people have dementia? ed.
6. Alzheimer's A (2011) 2011 Alzheimer's disease facts and figures. Alzheimer's & dementia : The Journal of the Alzheimer's Association 7: 208-244.
7. Miniño A, Xu J, Kochanek KD (2010) Deaths: preliminary data for 2008.: National Center for Health Statistics.
8. Alzheimer's_Association (2011) About Alzheimer's.
9. Reisberg B (1988) Functional assessment staging (FAST). Psychopharmacol Bull. pp. 653-659.
10. Schneider JA, Arvanitakis Z, Leurgans SE, Bennett DA (2009) The neuropathology of probable Alzheimer disease and mild cognitive impairment. Ann Neurol 66: 200-208.
11. Petersen RC, Smith GE, Waring SC, Ivnik RJ, Tangalos EG, et al. (1999) Mild Cognitive Impairment: Clinical Characterization and Outcome. pp. 303-308.
12. Selkoe DJ (2002) Deciphering the genesis and fate of amyloid beta-protein yields novel therapies for Alzheimer disease. J Clin Invest 110: 1375-1381.
13. Marien MR, Colpaert FC, Rosenquist AC (2004) Noradrenergic mechanisms in neurodegenerative diseases: a theory. Brain Res Brain Res Rev 45: 38-78.
14. Querfurth HW, LaFerla FM (2010) Alzheimer's Disease. pp. 329-344.
15. Glenner GG, Wong CW (1984) Alzheimer's disease: Initial report of the purification and characterization of a novel cerebrovascular amyloid protein. Biochemical and Biophysical Research Communications 120: 885-890.
16. Ittner LM, Götz J (2011) Amyloid-beta and tau - a toxic pas de deux in Alzheimer's disease. Nat Rev Neurosci 12: 67-72.
17. Kang J, Lemaire HG, Unterbeck A, Salbaum JM, Masters CL, et al. (1987) The precursor of Alzheimer's disease amyloid A4 protein resembles a cell-surface receptor. Nature 325: 733-736.
18. Ling Y, Morgan K, Kalsheker N (2003) Amyloid precursor protein (APP) and the biology of proteolytic processing: relevance to Alzheimer's disease. Int J Biochem Cell Biol 35: 1505-1535.
19. LaFerla FM, Green KN, Oddo S (2007) Intracellular amyloid-beta in Alzheimer's disease. Nat Rev Neurosci 8: 499-509.
20. Cam JA, Bu G (2006) Modulation of beta-amyloid precursor protein trafficking and processing by the low density lipoprotein receptor family. Mol Neurodegener 1: 8.
21. Wolfe MS (2009) Intramembrane proteolysis. Chem Rev 109: 1599-1612.
22. Mullan M, Crawford F, Axelman K, Houlden H, Lilius L, et al. (1992) A pathogenic mutation for probable Alzheimer's disease in the APP gene at the N-terminus of beta-amyloid. Nat Genet 1: 345-347.

23. Goate A, Chartier-Harlin MC, Mullan M, Brown J, Crawford F, et al. (1991) Segregation of a missense mutation in the amyloid precursor protein gene with familial Alzheimer's disease. Nature 349: 704-706.
24. Bekris LM, Yu C-E, Bird TD, Tsuang DW (2010) Review Article: Genetics of Alzheimer Disease. pp. 213-227.
25. Cruts M, Van Broeckhoven C (1998) Presenilin mutations in Alzheimer's disease. Human Mutation 11: 183-190.
26. AD&FTDMDB http://www.molgen.ua.ac.be/ADMutations.
27. Suzuki N, Cheung TT, Cai XD, Odaka A, Otvos L, Jr., et al. (1994) An increased percentage of long amyloid beta protein secreted by familial amyloid beta protein precursor (beta APP717) mutants. Science 264: 1336-1340.
28. Thal DR, Rub U, Schultz C, Sassin I, Ghebremedhin E, et al. (2000) Sequence of Abeta-protein deposition in the human medial temporal lobe. J Neuropathol Exp Neurol 59: 733-748.
29. German DC, Manaye KF, White CL, 3rd, Woodward DJ, McIntire DD, et al. (1992) Disease-specific patterns of locus coeruleus cell loss. Ann Neurol 32: 667-676.
30. Weinshenker D (2008) Functional consequences of locus coeruleus degeneration in Alzheimer's disease. Curr Alzheimer Res 5: 342-345.
31. Adolfsson R, Gottfries CG, Roos BE, Winblad B (1979) Changes in the brain catecholamines in patients with dementia of Alzheimer type. Br J Psychiatry 135: 216-223.
32. Mann DM, Lincoln J, Yates PO, Stamp JE, Toper S (1980) Changes in the monoamine containing neurones of the human CNS in senile dementia. Br J Psychiatry 136: 533-541.
33. Grudzien A, Shaw P, Weintraub S, Bigio E, Mash DC, et al. (2007) Locus coeruleus neurofibrillary degeneration in aging, mild cognitive impairment and early Alzheimer's disease. Neurobiol Aging 28: 327-335.
34. Zarow C, Lyness SA, Mortimer JA, Chui HC (2003) Neuronal loss is greater in the locus coeruleus than nucleus basalis and substantia nigra in Alzheimer and Parkinson diseases. Arch Neurol 60: 337-341.
35. Bondareff W, Mountjoy CQ, Roth M, Rossor MN, Iversen LL, et al. (1987) Neuronal degeneration in locus ceruleus and cortical correlates of Alzheimer disease. Alzheimer Dis Assoc Disord 1: 256-262.
36. Braak H, Del Tredici K (2011) The pathological process underlying Alzheimer's disease in individuals under thirty. Acta Neuropathol 121: 171-181.
37. Braak H, Del Tredici K (2011) Alzheimer's pathogenesis: is there neuron-to-neuron propagation? Acta Neuropathol 121: 589-595.
38. Heneka MT, Ramanathan M, Jacobs AH, Dumitrescu-Ozimek L, Bilkei-Gorzo A, et al. (2006) Locus ceruleus degeneration promotes Alzheimer pathogenesis in amyloid precursor protein 23 transgenic mice. J Neurosci 26: 1343-1354.
39. Pugh PL, Vidgeon-Hart MP, Ashmeade T, Culbert AA, Seymour Z, et al. (2007) Repeated administration of the noradrenergic neurotoxin N-(2-chloroethyl)-N-ethyl-2-bromobenzylamine (DSP-4) modulates neuroinflammation and amyloid plaque load in mice bearing amyloid precursor protein and presenilin-1 mutant transgenes. J Neuroinflammation 4: 8.
40. Franklin KBJ, Paxinos G (2007) The Mouse Brain in Stereotaxic Coordinates. New York, NY: Academic Press 351 p.
41. German DC, Walker BS, Manaye K, Smith WK, Woodward DJ, et al. (1988) The human locus coeruleus: computer reconstruction of cellular distribution. J Neurosci 8: 1776-1788.
42. Baker KG, Tork I, Hornung JP, Halasz P (1989) The human locus coeruleus complex: an immunohistochemical and three dimensional reconstruction study. Exp Brain Res 77: 257-270.
43. Halliday G (2004) Substantia Nigra and Locus Coeruleus. The Human Nervous System III Brain Stem and Cerebellum Second ed. USA: Elsevier.

44. Chan-Palay V, Asan E (1989) Quantitation of catecholamine neurons in the locus coeruleus in human brains of normal young and older adults and in depression. J Comp Neurol 287: 357-372.
45. Mouton PR, Pakkenberg B, Gundersen HJ, Price DL (1994) Absolute number and size of pigmented locus coeruleus neurons in young and aged individuals. J Chem Neuroanat 7: 185-190.
46. Lu W, Jaatinen P, Rintala J, Sarviharju M, Kiianmaa K, et al. (1997) Effects of lifelong ethanol consumption on rat locus coeruleus. Alcohol Alcohol 32: 463-470.
47. Riihioja P, Jaatinen P, Haapalinna A, Kiianmaa K, Hervonen A (1999) Effects of ageing and intermittent ethanol exposure on rat locus coeruleus and ethanol-withdrawal symptoms. Alcohol Alcohol 34: 706-717.
48. Rintala J, Jaatinen P, Wei L, Sarviharju M, Eriksson P, et al. (1998) Lifelong ethanol consumption and loss of locus coeruleus neurons in AA and ANA rats. Alcohol 16: 243-248.
49. Sara SJ (2009) The locus coeruleus and noradrenergic modulation of cognition. Nat Rev Neurosci 10: 211-223.
50. Koob GF (2008) A role for brain stress systems in addiction. Neuron 59: 11-34.
51. Aston-Jones G, Cohen JD (2005) An integrative theory of locus coeruleus-norepinephrine function: Adaptive gain and optimal performance. Annual Review of Neuroscience. Palo Alto: Annual Reviews. pp. 403-450.
52. Feinstein DL, Heneka MT, Gavrilyuk V, Dello Russo C, Weinberg G, et al. (2002) Noradrenergic regulation of inflammatory gene expression in brain. Neurochem Int 41: 357-365.
53. Iadecola C (2004) Neurovascular regulation in the normal brain and in Alzheimer's disease. Nat Rev Neurosci 5: 347-360.
54. Rogers J, Cooper NR, Webster S, Schultz J, McGeer PL, et al. (1992) Complement activation by beta-amyloid in Alzheimer disease. Proc Natl Acad Sci U S A 89: 10016-10020.
55. Heneka MT, Nadrigny F, Regen T, Martinez-Hernandez A, Dumitrescu-Ozimek L, et al. (2010) Locus ceruleus controls Alzheimer's disease pathology by modulating microglial functions through norepinephrine. Proc Natl Acad Sci U S A 107: 6058-6063.
56. Castren E, Thoenen H, Lindholm D (1995) Brain-derived neurotrophic factor messenger RNA is expressed in the septum, hypothalamus and in adrenergic brain stem nuclei of adult rat brain and is increased by osmotic stimulation in the paraventricular nucleus. Neuroscience 64: 71-80.
57. Xu ZQ, Shi TJ, Hokfelt T (1998) Galanin/GMAP- and NPY-like immunoreactivities in locus coeruleus and noradrenergic nerve terminals in the hippocampal formation and cortex with notes on the galanin-R1 and -R2 receptors. J Comp Neurol 392: 227-251.
58. Koylu EO, Smith Y, Couceyro PR, Kuhar MJ (1999) CART peptides colocalize with tyrosine hydroxylase neurons in rat locus coeruleus. Synapse 31: 309-311.
59. Warnecke M, Oster H, Revelli JP, Alvarez-Bolado G, Eichele G (2005) Abnormal development of the locus coeruleus in Ear2(Nr2f6)-deficient mice impairs the functionality of the forebrain clock and affects nociception. Genes Dev 19: 614-625.
60. Gotz J, Streffer JR, David D, Schild A, Hoerndli F, et al. (2004) Transgenic animal models of Alzheimer's disease and related disorders: histopathology, behavior and therapy. Mol Psychiatry 9: 664-683.
61. Casas C, Sergeant N, Itier JM, Blanchard V, Wirths O, et al. (2004) Massive CA1/2 neuronal loss with intraneuronal and N-terminal truncated Abeta42 accumulation in a novel Alzheimer transgenic model. Am J Pathol 165: 1289-1300.
62. Bayer TA, Wirths O (2008) Review on the APP/PS1KI mouse model: intraneuronal Abeta accumulation triggers axonopathy, neuron loss and working memory impairment. Genes Brain Behav 7 Suppl 1: 6-11.

63. Wirths O, Breyhan H, Schafer S, Roth C, Bayer TA (2008) Deficits in working memory and motor performance in the APP/PS1ki mouse model for Alzheimer's disease. Neurobiol Aging 29: 891-901.
64. Hsiao K, Chapman P, Nilsen S, Eckman C, Harigaya Y, et al. (1996) Correlative memory deficits, Abeta elevation, and amyloid plaques in transgenic mice. Science 274: 99-102.
65. Jung JH, An K, Kwon OB, Kim HS, Kim JH (2011) Pathway-specific alteration of synaptic plasticity in Tg2576 mice. Mol Cells 32: 197-201.
66. Oakley H, Cole SL, Logan S, Maus E, Shao P, et al. (2006) Intraneuronal beta-amyloid aggregates, neurodegeneration, and neuron loss in transgenic mice with five familial Alzheimer's disease mutations: potential factors in amyloid plaque formation. J Neurosci 26: 10129-10140.
67. Kalinin S, Polak PE, Lin SX, Sakharkar AJ, Pandey SC, et al. (2011) The noradrenaline precursor L-DOPS reduces pathology in a mouse model of Alzheimer's disease. Neurobiol Aging.
68. Calhoun ME, Wiederhold KH, Abramowski D, Phinney AL, Probst A, et al. (1998) Neuron loss in APP transgenic mice. Nature 395: 755-756.
69. German DC, Nelson O, Liang F, Liang CL, Games D (2005) The PDAPP mouse model of Alzheimer's disease: locus coeruleus neuronal shrinkage. J Comp Neurol 492: 469-476.
70. O'Neil JN, Mouton PR, Tizabi Y, Ottinger MA, Lei DL, et al. (2007) Catecholaminergic neuronal loss in locus coeruleus of aged female dtg APP/PS1 mice. J Chem Neuroanat 34: 102-107.
71. Citron M, Oltersdorf T, Haass C, McConlogue L, Hung AY, et al. (1992) Mutation of the beta-amyloid precursor protein in familial Alzheimer's disease increases beta-protein production. Nature 360: 672-674.
72. Cai XD, Golde TE, Younkin SG (1993) Release of excess amyloid beta protein from a mutant amyloid beta protein precursor. Science 259: 514-516.
73. Jankowsky JL, Slunt HH, Ratovitski T, Jenkins NA, Copeland NG, et al. (2001) Co-expression of multiple transgenes in mouse CNS: a comparison of strategies. Biomolecular Engineering 17: 157-165.
74. Thomas SA, Marck BT, Palmiter RD, Matsumoto AM (1998) Restoration of norepinephrine and reversal of phenotypes in mice lacking dopamine beta-hydroxylase. J Neurochem 70: 2468-2476.
75. Theron CN, de Villiers AS, Taljaard JJ (1993) Effects of DSP-4 on monoamine and monoamine metabolite levels and on beta adrenoceptor binding kinetics in rat brain at different times after administration. Neurochem Res 18: 1321-1327.
76. Szot P, Miguelez C, White SS, Franklin A, Sikkema C, et al. (2010) A comprehensive analysis of the effect of DSP4 on the locus coeruleus noradrenergic system in the rat. Neuroscience 166: 279-291.
77. Fritschy JM, Grzanna R (1992) Restoration of ascending noradrenergic projections by residual locus coeruleus neurons: compensatory response to neurotoxin-induced cell death in the adult rat brain. J Comp Neurol 321: 421-441.
78. Meissner WG, Frasier M, Gasser T, Goetz CG, Lozano A, et al. (2011) Priorities in Parkinson's disease research. Nat Rev Drug Discov 10: 377-393.
79. Mizuno Y, Hattori N, Kubo S, Sato S, Nishioka K, et al. (2008) Progress in the pathogenesis and genetics of Parkinson's disease. Philos Trans R Soc Lond B Biol Sci 363: 2215-2227.
80. Lewy FH (1912) Paralysis agitans, I. Pathologische Anatomie. Handbuch des Neurologie, herausgegeben von Lewndowsky, 3ter Band, Spezielle Pathologie IIs. Berlin, Germany: Springer. pp. 920-933.
81. Dawson TM, Ko HS, Dawson VL (2010) Genetic Animal Models of Parkinson's Disease. Neuron 66: 646-661.
82. Björklund A, Dunnett SB (2007) Dopamine neuron systems in the brain: an update. Trends in Neurosciences 30: 194-202.

83. Grace AA, Floresco SB, Goto Y, Lodge DJ (2007) Regulation of firing of dopaminergic neurons and control of goal-directed behaviors. Trends in Neurosciences 30: 220-227.
84. Iversen SD, Iversen LL (2007) Dopamine: 50 years in perspective. Trends in Neurosciences 30: 188-193.
85. Bello NT, Hajnal A (2010) Dopamine and binge eating behaviors. Pharmacol Biochem Behav 97: 25-33.
86. Koob GF, Volkow ND (2010) Neurocircuitry of addiction. Neuropsychopharmacology 35: 217-238.
87. Abeliovich A, Schmitz Y, Farinas I, Choi-Lundberg D, Ho WH, et al. (2000) Mice lacking alpha-synuclein display functional deficits in the nigrostriatal dopamine system. Neuron 25: 239-252.
88. Kahle PJ, Haass C, Kretzschmar HA, Neumann M (2002) Structure/function of alpha-synuclein in health and disease: rational development of animal models for Parkinson's and related diseases. J Neurochem 82: 449-457.
89. Eliezer D, Kutluay E, Bussell R, Jr., Browne G (2001) Conformational properties of alpha-synuclein in its free and lipid-associated states. J Mol Biol 307: 1061-1073.
90. Lee VM, Trojanowski JQ (2006) Mechanisms of Parkinson's disease linked to pathological alpha-synuclein: new targets for drug discovery. Neuron 52: 33-38.
91. Simon-Sanchez J, Schulte C, Bras JM, Sharma M, Gibbs JR, et al. (2009) Genome-wide association study reveals genetic risk underlying Parkinson's disease. Nat Genet 41: 1308-1312.
92. Lee MK, Stirling W, Xu Y, Xu X, Qui D, et al. (2002) Human alpha-synuclein-harboring familial Parkinson's disease-linked Ala-53 --> Thr mutation causes neurodegenerative disease with alpha-synuclein aggregation in transgenic mice. Proc Natl Acad Sci U S A 99: 8968-8973.
93. Fernagut PO, Chesselet MF (2004) Alpha-synuclein and transgenic mouse models. Neurobiol Dis 17: 123-130.
94. Fleming SM, Fernagut PO, Chesselet MF (2005) Genetic mouse models of parkinsonism: strengths and limitations. NeuroRx 2: 495-503.
95. Terzioglu M, Galter D (2008) Parkinson's disease: genetic versus toxin-induced rodent models. Febs J 275: 1384-1391.
96. Chesselet MF (2008) In vivo alpha-synuclein overexpression in rodents: a useful model of Parkinson's disease? Exp Neurol 209: 22-27.
97. Volles MJ, Lansbury PT, Jr. (2007) Relationships between the sequence of alpha-synuclein and its membrane affinity, fibrillization propensity, and yeast toxicity. J Mol Biol 366: 1510-1522.
98. Outeiro TF, Lindquist S (2003) Yeast cells provide insight into alpha-synuclein biology and pathobiology. Science 302: 1772-1775.
99. Chen L, Feany MB (2005) Alpha-synuclein phosphorylation controls neurotoxicity and inclusion formation in a Drosophila model of Parkinson disease. Nat Neurosci 8: 657-663.
100. Karpinar DP, Balija MB, Kugler S, Opazo F, Rezaei-Ghaleh N, et al. (2009) Pre-fibrillar alpha-synuclein variants with impaired beta-structure increase neurotoxicity in Parkinson's disease models. Embo J 28: 3256-3268.
101. Lashuel HA, Lansbury PT, Jr. (2006) Are amyloid diseases caused by protein aggregates that mimic bacterial pore-forming toxins? Q Rev Biophys 39: 167-201.
102. Reiserer RS, Harrison FE, Syverud DC, McDonald MP (2007) Impaired spatial learning in the APPSwe + PSEN1DeltaE9 bigenic mouse model of Alzheimer's disease. Genes Brain Behav 6: 54-65.
103. Schmitz C, Rutten BP, Pielen A, Schafer S, Wirths O, et al. (2004) Hippocampal neuron loss exceeds amyloid plaque load in a transgenic mouse model of Alzheimer's disease. Am J Pathol 164: 1495-1502.

104. Urbanc B, Cruz L, Le R, Sanders J, Ashe KH, et al. (2002) Neurotoxic effects of thioflavin S-positive amyloid deposits in transgenic mice and Alzheimer's disease. Proc Natl Acad Sci U S A 99: 13990-13995.
105. Mueller D, Cahill SP (2010) Noradrenergic modulation of extinction learning and exposure therapy. Behav Brain Res 208: 1-11.
106. Murchison CF, Zhang XY, Zhang WP, Ouyang M, Lee A, et al. (2004) A distinct role for norepinephrine in memory retrieval. Cell 117: 131-143.
107. Volianskis A, Kostner R, Molgaard M, Hass S, Jensen MS (2010) Episodic memory deficits are not related to altered glutamatergic synaptic transmission and plasticity in the CA1 hippocampus of the APPswe/PS1deltaE9-deleted transgenic mice model of ss-amyloidosis. Neurobiol Aging 31: 1173-1187.
108. Szapacs ME, Numis AL, Andrews AM (2004) Late onset loss of hippocampal 5-HT and NE is accompanied by increases in BDNF protein expression in mice co-expressing mutant APP and PS1. Neurobiol Dis 16: 572-580.
109. Gispert S, Del Turco D, Garrett L, Chen A, Bernard DJ, et al. (2003) Transgenic mice expressing mutant A53T human alpha-synuclein show neuronal dysfunction in the absence of aggregate formation. Mol Cell Neurosci 24: 419-429.
110. Rockenstein E, Mallory M, Hashimoto M, Song D, Shults CW, et al. (2002) Differential neuropathological alterations in transgenic mice expressing alpha-synuclein from the platelet-derived growth factor and Thy-1 promoters. J Neurosci Res 68: 568-578.
111. Daher JP, Ying M, Banerjee R, McDonald RS, Hahn MD, et al. (2009) Conditional transgenic mice expressing C-terminally truncated human alpha-synuclein (alphaSyn119) exhibit reduced striatal dopamine without loss of nigrostriatal pathway dopaminergic neurons. Mol Neurodegener 4: 34.
112. Backman CM, Malik N, Zhang Y, Shan L, Grinberg A, et al. (2006) Characterization of a mouse strain expressing Cre recombinase from the 3' untranslated region of the dopamine transporter locus. Genesis 44: 383-390.
113. Diaz-Ruiz O, Zapata A, Shan LF, Zhang YJ, Tomac AC, et al. (2009) Selective Deletion of PTEN in Dopamine Neurons Leads to Trophic Effects and Adaptation of Striatal Medium Spiny Projecting Neurons. Plos One 4: 13.
114. Bello EP, Mateo Y, Gelman DM, Noain D, Shin JH, et al. (2011) Cocaine supersensitivity and enhanced motivation for reward in mice lacking dopamine D(2) autoreceptors. Nature Neuroscience 14: 1033-U1128.
115. Lein ES, Hawrylycz MJ, Ao N, Ayres M, Bensinger A, et al. (2007) Genome-wide atlas of gene expression in the adult mouse brain. Nature 445: 168-176.
116. Crawley JN (2007) Motor Functions. What's wrong with my mouse? Behavioral phenotyping of transgenic and knockout mice. Second ed. N.Y.: John Wiley & Sons, Inc. .
117. Colwell CS (2011) Linking neural activity and molecular oscillations in the SCN. Nat Rev Neurosci advance online publication.
118. Liebetanz D, Baier PC, Paulus W, Meuer K, Bahr M, et al. (2007) A highly sensitive automated complex running wheel test to detect latent motor deficits in the mouse MPTP model of Parkinson's disease. Exp Neurol 205: 207-213.
119. Fleming SM, Tetreault NA, Mulligan CK, Hutson CB, Masliah E, et al. (2008) Olfactory deficits in mice overexpressing human wildtype alpha-synuclein. Eur J Neurosci 28: 247-256.
120. Borchelt DR, Ratovitski T, van Lare J, Lee MK, Gonzales V, et al. (1997) Accelerated amyloid deposition in the brains of transgenic mice coexpressing mutant presenilin 1 and amyloid precursor proteins. Neuron 19: 939-945.
121. Sun A, Nguyen XV, Bing G (2002) Comparative analysis of an improved thioflavin-s stain, Gallyas silver stain, and immunohistochemistry for neurofibrillary tangle demonstration on the same sections. J Histochem Cytochem 50: 463-472.

122. Guntern R, Bouras C, Hof PR, Vallet PG (1992) An improved thioflavine S method for staining neurofibrillary tangles and senile plaques in Alzheimer's disease. Experientia 48: 8-10.
123. Liu Y, Yoo MJ, Savonenko A, Stirling W, Price DL, et al. (2008) Amyloid pathology is associated with progressive monoaminergic neurodegeneration in a transgenic mouse model of Alzheimer's disease. J Neurosci 28: 13805-13814.
124. Thomas B, von Coelln R, Mandir AS, Trinkaus DB, Farah MH, et al. (2007) MPTP and DSP-4 susceptibility of substantia nigra and locus coeruleus catecholaminergic neurons in mice is independent of parkin activity. Neurobiol Dis 26: 312-322.
125. PerkinElmerCetus (1989) Amplifications: 2: 1-3.
126. Yaylaoglu MB, Titmus A, Visel A, Alvarez-Bolado G, Thaller C, et al. (2005) Comprehensive expression atlas of fibroblast growth factors and their receptors generated by a novel robotic in situ hybridization platform. Dev Dyn 234: 371-386.
127. Cankaya M, Hernandez AM, Ciftci M, Beydemir S, Ozdemir H, et al. (2007) An analysis of expression patterns of genes encoding proteins with catalytic activities. BMC Genomics 8: 232.

Acknowledgments

First of all I would like to thank Prof. Gregor Eichele for giving me the opportunity to join his lab and allowing me to pursue these projects. I am very thankful for all his support and the constructive discussions.

I would like to thank my thesis committee members, Prof. Dr. med. Mathias Bähr and Prof. Dr. Ahmed Mansouri for their helpful suggestions and fruitful discussions throughout my PhD.

Thank you to additional members of my examination board: Prof. Dr. Markus Zweckstetter, Prof. Dr. Klaus-Armin Nave and Prof. Dr. André Fiala for very kindly accepting my invitation to join my examination board.

This work could have not been possible without the help of all my collaborators, many of whom are now also my friends. Prof. Dr. Michael Heneka and his lab, especially Dr. Thea Hammerschmidt, who contributed to the analyses of the Ear2/APP mice. The work on PD was a collaborative effort with Dr. Xunlei Zhou and Dr. Insa Geffers. Sharif Mahsur for electroporation of our construct. Inga Urban for help with the initial steps of characterization of the Ear2 mice.

Thank you to the wonderful animal care takers and staff of the BTL, especially to Denise Brödner, Ute Kuntze, Dr. Ulrike Teichmann.

For excellent technical assistance, support, their friendship and patience while I started speaking German, I would like to thank: Frauke Grabbe and Maren Brockmeyer.

Thank you to former lab members for all their support and help, Dr. Nora Szabó, Barbara Fischer, Dr. Xunlei Zhou, Dr. Judit Meyer-Kovac and Dr. Gonzalo Alvarez-Bolado.

Thank you to all members of the Genes and Behavior Dept. Specially to Helena Miletic (my life in the lab without her would just not work!), Chrisitne van den Bogaart, Inga Urban, Sibel Aktay, Dr. Insa Geffers, Dr. Johanna Barclay and Dr. Lars Geffers for making the lab a fun place and for all their support and help. Of course, Jana the most!

Thank you to all the mice who helped me contribute a small grain of sand to science.

To my Mexican friends who became my second family, Tania Garfias Macedo, Dr. Yara Mejia, Aldo Camacho Zarco. Gracias por el apoyo incondicional!

My greatest appreciation is to my family. For all their love, support and encouragement. Muchas gracias!

Last but not least to Darrin Miral for all his love, encouragement and support through all this years together. Amor, sin ti esto no estaria pasando. Muchisimas gracias por estar ahi siempre! PS. Posit is for you.

List of Abbreviations

6-OHDA	6-hydroxydopamine
AD	Alzheimer's disease
AICD	APP intracellular C-terminal domain
APP	Amyloid precursor protein
Aβ	Amyloid-beta
CAM	Chloramphenicol
CX	Cortex
DA	Dopamine
DOPS	L-threo-dihydroxyphenylserine
DSP-4	N-(2-chloroethyl)-N-ethyl-2-bromobenzylamine
FC	Frontal cortex
HC	Hippocampus
IVC	Individually ventilated cage
LC	Locus Coeruleus
MCI	Mild cognitive impairment
MPTP	1-methyl-4-phenyl1-1,2,3,6 tetrahydropyridine
NA	Noradrenaline
OB	Olfactory bulb
ORF	Open reading frame
PD	Parkinson's disease
PS1	Presenilin 1
SN	Substantia nigra
SPF	Specific pathogen free
Th	Tyrosine hydroxylase
VTA	Ventral tegmental area
wt	wild-type

Ana C. Martinez Hernandez
Theodor Heuss Str. 35
37075 Goettingen, Germany
+49 (0)176 2082-4946
amartin4@gwdg.de

EDUCATION

March 2008 – Present: PHD CANDIDATE
Topic: New genetic mouse models for neurodegenerative diseases: Contribution of noradrenaline to Alzheimer's disease pathogenesis and creation of a new genetic model for Parkinson's disease.
Goettingen Graduate School for Neuroscience and Molecular Biosciences, Max Planck Institute for Biophysical Chemistry, Goettingen, Germany

October 2003: BACCALAUREATE OF SCIENCE, HONOURS
Major: Molecular Biology and Genetics
University of Guelph, Guelph, Ontario, Canada

RESEARCH EXPERIENCE

May 2004 – March 2008: TECHNICAL COORDINATOR / TECHNICAL ASSISTANT
Max Planck Institute of Experimental Endocrinology, for Biophysical Chemistry
Hannover and Goettingen, Germany

January 2004 – April 2004: LABORATORY RESEARCH ASSISTANT
Biomedical Sciences Department
University of Guelph, Guelph, Ontario, Canada

April 2003 – December 2003: LABORATORY RESEARCH ASSISTANT
Biomedical Sciences Department
University of Guelph, Guelph, Ontario, Canada

May 2000 – August 2000: LABORATORY RESEARCH INTERN
Dept. of Microbiology and Dept. of Molecular Biology and Genetics
Michigan State University, East Lansing, Michigan, USA

PUBLICATIONS

Diez-Roux G, Banfi S, Sultan M, Geffers L, Anand S, Rozado D, Magen A, Canidio E, Pagani M, Peluso I, Lin-Marq N, Koch M, Bilio M, Cantiello I, Verde R, De Masi C, Bianchi SA, Cicchini J, Perroud E, Mehmeti S, Dagand E, Schrinner S, Nurnberger A, Schmidt K, Metz K, Zwingmann C, Brieske N, Springer C, **Hernandez AM**, Herzog S, Grabbe F, Sieverding C, Fischer B, Schrader K, Brockmeyer M, Dettmer S, Helbig C, Alunni V, Battaini MA, Mura C, Henrichsen CN, Garcia-Lopez R, Echevarria D, Puelles E, Garcia-Calero E, Kruse S, Uhr M, Kauck C, Feng G, Milyaev N, Ong CK, Kumar L, Lam M, Semple CA, Gyenesei A, Mundlos S, Radelof U, Lehrach H, Sarmientos P, Reymond A, Davidson DR, Dolle P, Antonarakis SE, Yaspo ML, Martinez S, Baldock RA, Eichele G, Ballabio A: **A high-resolution anatomical atlas of the transcriptome in the mouse embryo**. *PLoS Biol* 2011, **9**(1):e1000582.

Heneka MT, Nadrigny F, Regen T, **Martinez-Hernandez A**, Dumitrescu-Ozimek L, Terwel D, Jardanhazi-Kurutz D, Walter J, Kirchhoff F, Hanisch UK, Kummer MP: **Locus ceruleus controls Alzheimer's disease pathology by modulating microglial functions through norepinephrine**. *Proc Natl Acad Sci U S A* 2010, **107**(13):6058-6063.

Cankaya M, **Hernandez AM**, Ciftci M, Beydemir S, Ozdemir H, Budak H, Gulcin I, Comakli V, Emircupani T, Ekinci D, Kuzu M, Jiang Q, Eichele G, Kufrevioglu OI: **An analysis of expression patterns of genes encoding proteins with catalytic activities**. *BMC Genomics* 2007, **8**:232.

POSTER PRESENTATIONS

March 2011 **NORADRENALINE LEVELS IN THE BRAIN THROUGH AGING IN A NOVEL MODEL OF AD WITH A REDUCED LC,** Meeting on neuroinflammation, Bonn, Germany

November 2009 **CONSEQUENCES OF NORADRENALINE DEFICITS IN A NOVEL MODEL OF ALZHEIMER'S DISEASE,** GGNB Science Day, Goettingen, Germany

March 2004 **IGF-II-MEDIATED SIGNALING IN BREAST CANCER AND NORMAL MAMMARY EPITHELIAL CELLS,** American Association for Cancer Research Annual Meeting, Florida, USA